OPEN ACCESS

University of Dundee

University of Dundee

Nano-topography

Giannini, Marianna; Primerano, Chiara; Berger, Liron; Giannaccini, Martina; Wang, Zhigang; Landi, Elena

Link to publication in Discovery Research Portal

Corresponding Author: Professor Vittoria Raffa, PhD

Corresponding Author's Institution: Università di Pisa

First Author: Marianna Giannini, PhD

Order of Authors: Marianna Giannini, PhD; Chiara Primerano; Liron
Berger, PhD; Martina Giannaccini, PhD; Zhigang Wang, PhD; Elena Landi,
PhD; Alfred Cuschieri, Prof; Luciana Dente, Prof; Giovanni Signore, PhD;
Vittoria Raffa, PhD

Abstract: The 3-D spatial and mechanical features of nano-topography can
create alternative environments, which influence cellular response. In
this paper, murine fibroblast cells were grown on surfaces characterized
by protruding nanotubes. Cells cultured on such nano-structured surface
exhibit stronger cellular adhesion compared to control groups but,
despite the fact that stronger adhesion is generally believed to promote
cell cycle progression, the time cells spend in G1 phase is doubled. This
apparent contradiction is solved by confocal microscopy analysis, which
shows that the nano-topography inhibits actin stress fiber formation. In
turn, this impairs RhoA activation, which is required to suppress the
inhibition of cell cycle progression imposed by p21/p27. This finding
suggests that the generation of stress fiber formation, required to
impose the homeostatic intracellular tension, rather than cell
adhesion/spreading is the limiting factor for cell cycle progression.
Indeed, nano-topography could represent a unique tool to inhibit
proliferation in adherent well-spread cells.
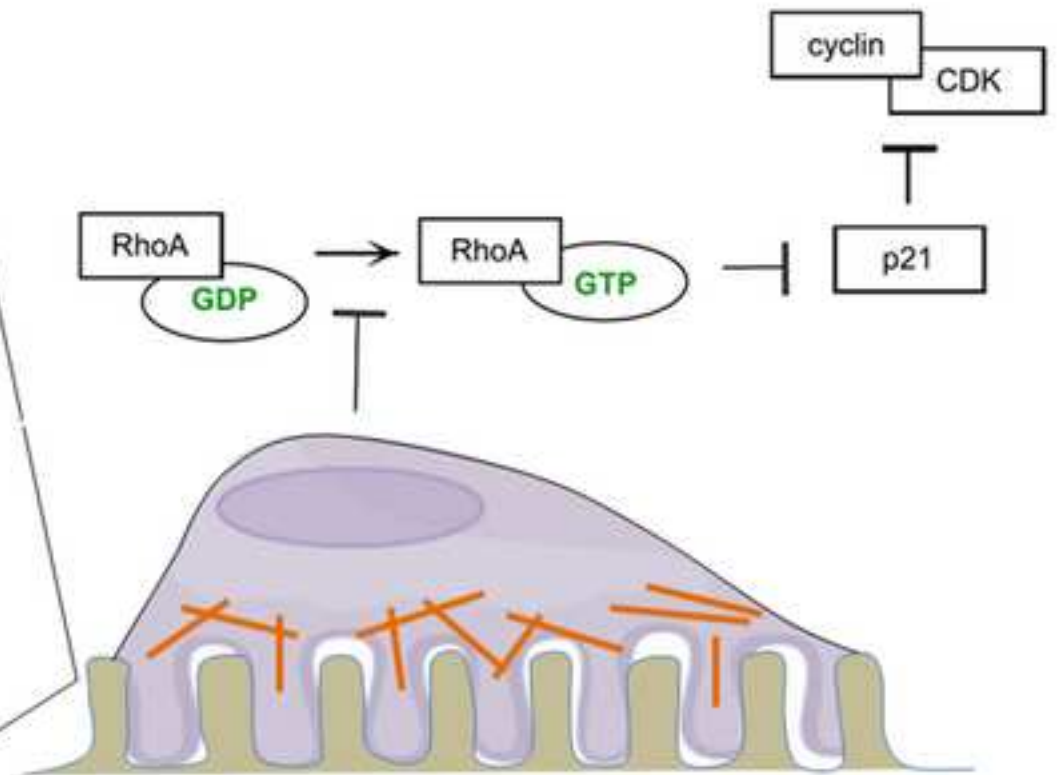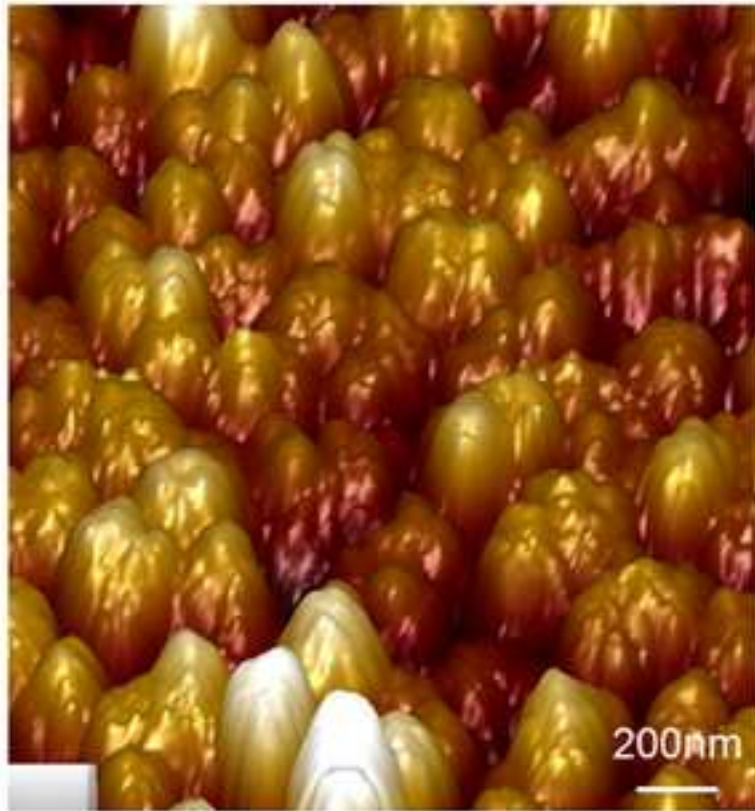
Nano-topography: quicksand for cell cycle progression?

Marianna Giannini, PhD[a], Chiara Primerano, MsC[a], Liron Berger, PhD[a], Martina Giannaccini, PhD[a], Zhigang Wang,

PhD[b], Elena Landi, PhD[a], Alfred Cuschieri, MD[b], Luciana Dente, MsC[a], Giovanni Signore, PhD[c,d], Vittoria Raffa, PhD[a]*

[a] Department of Biology, Università di Pisa, S.S. 12 Abetone e Brennero 4, Pisa 56127, Italy

[b] Institute for Medical Science and Technology, University of Dundee, 1, Wurzburg Loan, Dundee, DD2

1FD, United Kingdom

[c] Center for Nanotechnology Innovation @NEST, Istituto Italiano di Tecnologia, Piazza San Silvestro 12,

56127 Pisa, Italy

[d] NEST, Scuola Normale Superiore, and Istituto Nanoscienze-CNR, Piazza San Silvestro 12, 56127 Pisa,

Italy

*Corresponding author: vittoria.raffa@unipi.it

Marianna Giannini, marianna.giannini@sssup.it tel:00390502211487

Chiara Primerano, chiaraprim@gmail.com tel:00390502211487

Liron Berger, lirberger@gmail.com tel:00390502211487

Martina Giannaccini, martina.giannaccini@unipi.it tel:00390502211488

Zhigang Wang, z.z.wang@dundee.ac.uk +44 (0)1382 388357

Elena Landi, elena.landi@unipi.it +39 050 2211483

Alfred Cuschieri, a.cuschieri@dundee.ac.uk +44 (0)1382 388357

Luciana Dente, luciana.dente@unipi.it tel:00390502211488

Giovanni Signore, giovanni.signore@iit.it +39.050.509111

Vittoria Raffa vittoria.raffa@unipi.it   tel:00390502211487

Word count for abstract: 149

Word count for complete manuscript (to include body text and figure legends): 5135

Number of reference: 34

Number of figure: 8

ABSTRACT

The 3-D spatial and mechanical features of nano-topography can create alternative environments, which influence cellular response. In this paper, murine fibroblast cells were grown on surfaces characterized by protruding nanotubes. Cells cultured on such nano-structured surface exhibit stronger cellular adhesion compared to control groups but, despite the fact that stronger adhesion is generally believed to promote cell cycle progression, the time cells spend in G1 phase is doubled. This apparent contradiction is solved by confocal microscopy analysis, which shows that the nano-topography inhibits actin stress fiber formation. In turn, this impairs RhoA activation, which is required to suppress the inhibition of cell cycle progression imposed by p21/p27. This finding suggests that the generation of stress fiber formation, required to impose the homeostatic intracellular tension, rather than cell adhesion/spreading is the limiting factor for cell cycle progression. Indeed, nano-topography could represent a unique tool to inhibit proliferation in adherent well-spread cells.

KEYWORDS: nano-topography, cell cyle, RhoA, mechanotransduction

Introduction

The local mechanical interaction between the cell and its microenvironment is a mechanism influencing aspects of cell physiology and pathology [1].Mechanotransduction, i.e. the mechanisms by which cells sense, integrate, transmit and transduce mechanical stimuli into a biochemical response, is known to influence cell development [2], differentiation [3], migration [4], proliferation [5], tumor formation and progression [6]. Adherent cells probe their microenvironment and respond to the stiffness of the microenvironment by pulling on the extracellular matrix (ECM). Focal adhesions (FA) represent the bridge connecting the matrix to the cellular cytoskeleton [7]. Myosin-based contractility acts as a primary regulator of contractile forces responsible for pulling

2

the ECM. Indeed, this traction force is responsible of tensional homeostasis of the cell, which, in turn, has a role in regulating signaling pathways that are involved in fundamental cell processes [8, 9]. Cell adhesion and intracellular tension generation are obviously linked but occur through different pathways, which cross-talk, thereby influencing each other [10]. Key actors of these pathways are the small GTPase Rac, Cdc42 and RhoA [11]. The number of proteins found at point adhesions is large and many of them are mechanosensitive (MS) proteins. An important scaffold MS protein is the focal adhesion kinase (FAK), which is essential for dynamic adhesion (assembly/disassembly) [12]. Formation of a Src kinase-FAK complex is required to sustain Rac1 and Cdc42 activation while suppress RhoA, acting on the respective GAP and GEF. Rac1 and Cdc42 regulate nucleation, promoting the formation of filopodia and lamellipodia and cell spreading [13]. Cell spreading in turn, promotes aggregation of scaffold proteins and enlargement of the nascent FA, this process being positively regulated by the availability of adhesion molecules in the matrix. The resulting increase of force at the cell-matrix interface triggers RhoA activation and Rac1 and Cdc42 suppression [14]. RhoA promotes interaction of myosin II with actin filaments and acto-myosin contraction, which ultimately results in the formation of stress fibers, composed by longitudinally oriented actin filaments. Myosin II-generated intracellular tension induces conformational changes in various adhesion proteins, resulting in enhanced mechanotransduction and regulation of several signaling pathways. Matrix can influence both cell spreading by varying the availability of adhesion molecules, and intracellular tension generation by dissipating the myosin II-generated force. The current literature provides information on how cells respond to the change of matrix properties. Generally, cells cultured on rigid surfaces coated with high densities of ECM proteins exhibit large, myosin II-dependent, focal adhesions, whereas cells grown on compliant substrates coated with low densities of adhesion molecules tend to have smaller adhesions [15].

3

Mechanical signaling from cell adhesions regulates several processes, including cell proliferation [5, 16]. Under normal homeostatic tension, the cell proliferates at normal levels. Alterations of substrate stiffness and cell/matrix interaction induce a change in homeostatic tension and consequently, a cellular response. When the stiffness of the microenvironment is abnormally low, cells will not adhere or remain round-shaped, do not proliferate and activate the apoptotic program. By contrast, if matrix stiffness is abnormally high, cell adhesion, tensional homeostasis and intracellular contractility abnormally increase, resulting in aberrant expression of genes, which are important for cell proliferation [5]. In 2-D scaffolds, the density of adhesion molecules seems to be the limiting factor and cell spreading but not necessarily acto-myosin contraction remains tightly coupled with proliferation [17]. Cell proliferation is thus commonly associated with cell spreading (rounded-shaped cells associated with low proliferation, whereas well-spread cells associated with high proliferation [18]). In the present study, we use a 3-D scaffold formed by vertically aligned nanostructures protruding from the surface and demonstrate that the density of adhesion molecules is not a limiting factor. In fact, the nano-topography causes a 5 fold increase of the available surface area for coating, creating a permissive environment, which strongly enhances cell attachment. However, as the protruding nanostructures are flexible, they can potentially bend and dissipate the applied mechanical force when loaded. This substrate offers a unique microenvironment, combining high exposed area, which improves cellular adhesion, with compliance, which mechanically inhibits stress fiber formation and cell contractility. Indeed, our results suggest that the generation of stress fibers and intracellular tension is the limiting factor for cell cycle progression, even in presence of strong cell adhesion.

Methods

Synthesis of nanostructured surface

4

Anodic aluminium oxide filtration membranes (Whatman, Anodisc, diameter 47 mm or 13 mm, thickness 60 μm; pore diameter 200 nm) have been used as a template which provides a matrix of uniformly distributed through holes. The holes have been filled with barium titanate, accordingly to a well consolidated protocol [19, 20]. Briefly, ammonium hexafluorotitanate (($NH_4)_2TiF_6$ 10 mM, Sigma-Aldrich Co) and barium nitrate ($Ba(NO_3)_2$ 10 mM, Sigma-Aldrich Co) were dissolved in aqueous solution of boric acid (30 mM, Sigma-Aldrich Co) at room temperature. The pH was adjusted to 2.0 by adding 6 M HCl drop wise. The template membranes were vertically immersed in the precursor solutions and held at 60°C in a bath for 20 h. The membranes were then removed from the solutions and extensively rinsed. The protocol provides a nanostructured surface which we have deeply characterised in a previous work [19]. Briefly, the holes are filled with amorphous $BaTiO_3$, as demonstrated by electron microscopy, EDX microanalysis and X-ray powder diffraction [19]. The $BaTiO_3$ has the shape of vertically aligned nanotubes, which protrude few hundred of nanometres from the template, providing a nano-topography, as deeply characterised by atomic force microscopy (peak-to-peak height of 236± 58 nm [19]).

AFM

T or T-NT were placed onto the atomic force microscopy (AFM) stage and imaged using ScanAsyst Adaptive mode on the Bioscope Catalyst (Bruker). Roughness was measured via the Nanoscope Analysis Software.

Cell lines

The NIH-3T3 murine fibroblast cell line (ATCC) was cultured at 37°C with 5% CO_2 in Dulbecco's Modified Eagle's Medium (DMEM) containing 10% heat inactivated foetal bovine serum (FBS), 2mM L-glutamine, 100 IU ml^{-1} penicillin, 100 μg ml^{-1} streptomycin and 0.75 μg ml^{-1} amphotericin-B. The FAK$^{-/-}$ mouse embryonic cells (MEF) derived from FAK knockout mouse were kindly donated from Prof S. Hanks and Dr L.S. Ryzhova. We

received two clones: tet-FAK cells inducibly expressing wild type FAK and tet-FAK cells inducibly expressing mutant FAK (F397) [21]. Cell were cultured at 37°C with 5% CO_2 in DMEM high glucose containing 10% heat inactivated FBS, 2 mM L-glutamine, 1 mM sodium pyruvate, 100 IU ml^{-1} penicillin, 100 µg ml^{-1} streptomycin and 0.75 µg ml^{-1} amphotericin-B and tetracycline 1 µg ml^{-1} to keep expression off.

Cultures plastic (K), T and T-NT were coated with poly-L-lysine (PLL) (Sigma-Aldrich Co) or fibronectin (FN) 10 µg ml^{-1} in PBS. 24 h after cell seeding, T or T-NT substrates were moved in new dishes, in order to exclude from the analysis cells adhering on the bottom of the well. Fibroblasts were seeded at a density of $2.5 \cdot 10^4$ per cm^2 on K, T or T-NT.

Cytochemistry

Anti-p-histone H3 (Upstate Biotechnology), EdU staining (Click-iT EdU imaging kit, Life Technologies) and actin staining (R415, Life Technologies) were performed according to the manufacturer's instructions and analysed by optical or confocal microscopy (additional information in supplementary materials) 72 h, 24 h and 24 h after cell seeding, respectively.

Total RhoA and active RhoA

Cells were starved for 24 h in Optimem (Gibco). One hour after incubation with DMEM containing 10% FBS, cells were lysed and protein were extracted and chilled in N_2. After normalization of protein concentration, quantification of total RhoA (BK150, Cytoskeleton Inc.) and active RhoA (BK124, Cytoskeleton Inc.) was performed in the same lysates.

Scanning electron microscopy (SEM)

Electron imaging was performed with a scanning electron microscope (FEI XL20) equipped with Energy Dispersive X-ray spectrometer (EDX, EDAC model). For cell imaging, after 24 h of incubation, the cells were washed with PBS, fixed with formaldehyde 4% for 15 min, dehydrated via 5 min immersions in increasing concentrations of methanol 30% (x2), 50% (x2), 70% (x2) and 90% (x2), followed by

6

further dehydration with anhydrous MeOH and then T and T-NT membranes were allowed to dry overnight at room temperature.

Confocal analysis

Each experiment was conducted in triplicate and high resolution images (512x512 pixels) were acquired by confocal microscopy (DAPI channel and TRITC channel). 20-25 cells per sample were analysed by Fiji software. For each cell, the cell boundary was automatically calculated via Fiji (wand tracing tool), setting the threshold level (over/under) corresponding to a clear background (TRITC image). For each cell, we calculated the area, the centre of mass, the maxFeret, the minFeret and angle Feret of the nucleus (from DAPI image) and the area, the centre of mass, the maxFeret, the minFeret, angle Feret and the directionality ("directionality" plugin) of the cell boundary (from TRITC image). The maxFeret and the minFeret are the longest and the shortest distance between any two points along the cell/nucleus boundary, respectively. The angle Feret is the angle between the maxFeret axis and the reference system. The software output of the "directionality" plugin is the directionality histograms, indicating the amount of actin staining in a given direction. The plugin generates statistics on the highest peak found, which is fitted by a Gaussian function. Cell elongation was calculated as ratio between the maxFeret and the minFeret of the ROI corresponding to the cell boundary.

Cytofluorimetry

Twenty-four hours after cell seeding, EdU was added to the cell culture medium and cells were incubated at 37°C for 18 h. The cells were detached by trypsinization and 10^6 cells per sample were centrifuged. Cell pellet was re-suspended in 100 µl of 4% paraformaldehyde, incubated for 15 min at RT and then added with 3 ml of 1% BSA in PBS. Cells were centrifuged and the pellet was re-suspended with 100 µl of 0.05% Saponin in PBS and incubated at RT for 15 min. The cells were added with 3 ml of 1%

BSA in PBS and centrifuged. The pellet was resuspended in Alexa fluorazide solution and incubated at RT for 15 min. Then, the cells were added with 3ml of 0.05% Saponin in PBS and centrifuged. The cell pellet was re-suspended in 500 µl of RNase A solution (0.25 µg ml^{-1}) and kept in ice until reading in the flow cytometer (FACS scan, BD). 20,000 cells were read from each tube.

Real-time PCR

Twenty-four hours after cell seeding, total RNAs were extracted from 10^5 cells cultured on plastic (K), T or NT with RNeasy Micro Kit (Qiagen) accordingly to manufacturer protocol. cDNAs were obtained by RT-PCR using 200-500 ng RNA with QuantiTect Reverse Transcription kit (Qiagen) following manufacturer instruction (all reagents included). The resulting cDNA were diluted 1:50 up to 1:100 in nuclease-free water accordingly to initial RNA template concentration and stored in aliquots at -20°C. Real-time PCR was performed with PowerUp SYBR Green Master Mix (Applied Biosystems) on a Rotor-Gene 6000 (Corbett). Gene-specific primers were designed using Primer3 plus: GAPDH_Fwd CATGGCCTTCCGTGTTCCTA and Rev CCTGCTTCACCACCTTCTTGAT as internal control; Cdkn1A(p21)_Fwd CAGACCAGCCTGACAGATTTCTA and_Rev GAGGGCTAAGGCCGAAGATG; Cdkn1B(p27)_Fwd TCGACGCCAGACGTAAACAG and Rev AGGCAGATGGTTTAAGAGTGCC; Ccne1(CycE)_Fwd CCTTTCAGTCCGCTCCAGAA and Rev GGGATGAAAGAGCAGGGGTC. The relative gene expression level was determined by ΔΔCt method.

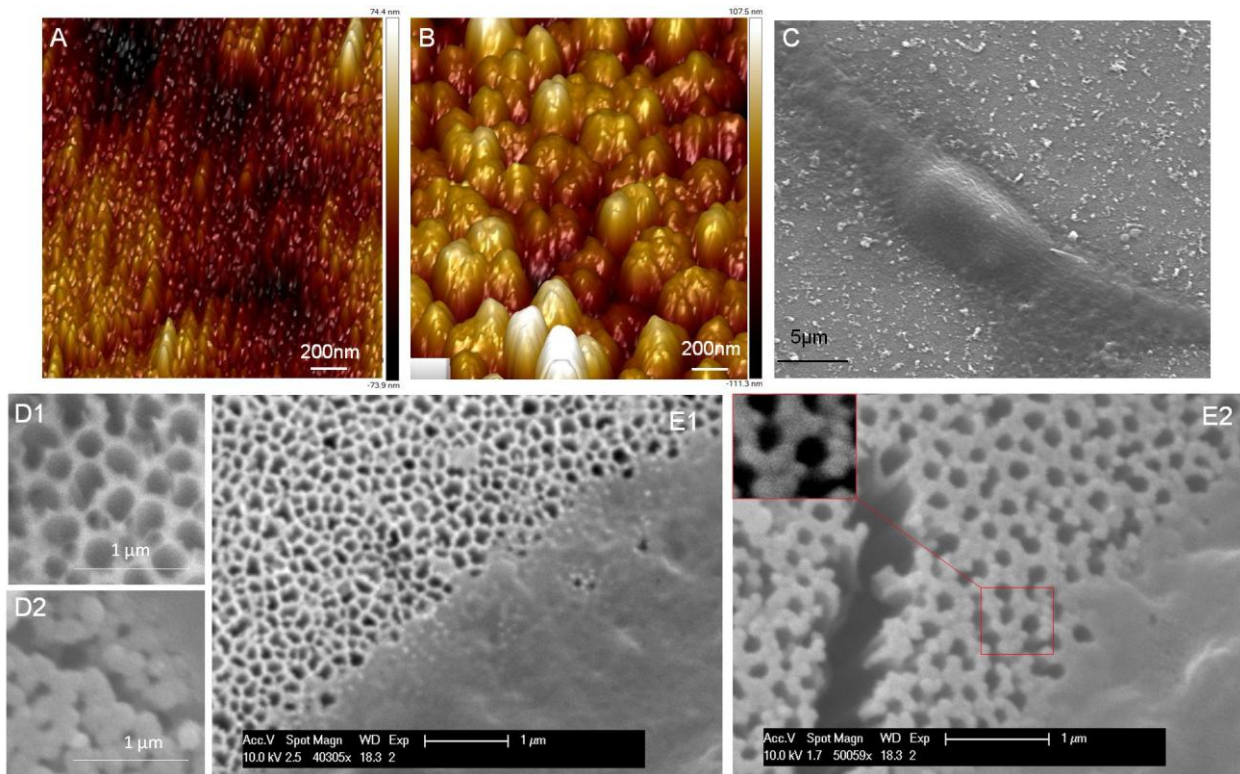One-way t-test was applied to compare the T-NT to T gene expression level normalized against control K.

Statistical analysis

8

Values are reported as the mean ± S.E.M. Significance was set at p≤0.05. Statistical analyses were performed with GraphPad Prism 6.0 version. ***, ### are p<0.001, **, ## p<0.01, *, # p<0.05. "n.s." indicates non-significance.

Results

The nano-topography enhances cell adhesion

The nano-structured surface is formed by an array of vertically aligned nanotubes (VANT) of barium titanate (Figure 1), a material largely used in biomedical implants [22]. The nanotubes are nano-structures, which protrude from the holes of a template membrane made by aluminium oxide (Figure 1D1 and 1D2) (extensive characterization provided in [19]). Briefly, the VANTs have a regular topography, i.e. single nanotubes with height 236 ± 58 nm (according to AFM imaging [19]) and a diameter of 180.76 ± 20.41 nm (according to SEM imaging, n=30). Figure 1E shows the morphology of the flat template (T) and the nano-structurated one (T-NT). The nanotubes seem to have a certain degree of flexibility, as shown in Figure 1E2, where the single tubes (inset) bend to cluster together, following the dehydration process. The VANTs offer a 5 fold increase of the superficial area compared to the flat template. Before the use, the flat template (T), the nanostructured one (T-NT) or the plastic controls (K) were coated with poly-L-lysine (PLL). We observed a strong adhesion of cells to the nanostructured substrate, i.e. a tenfold decrease of the ability of mechanical and chemical detachment of cells from T-NT, compared to controls (T and K). Specifically, after the detachment procedure, the percentage of cells detached from T-NT was $4.1 \pm 2.2\%$, while the percentage of cells detached from controls was $39.7 \pm 3.7\%$ and $36.6 \pm 2.3\%$ for K and T groups, respectively, reaching a high level of statistical significance (p<0.0001) [19]. Cells cultured on T-NT appear to be well-spread and tightly anchored the nano-structured surface (Figure 1C).

Figure 1. A) AFM image of the flat template T. B) AFM image of the nano-structured template T-NT. C) Low magnification image showing a NIH-3T3 cell cultured on T-NT. D) SEM imaging of empty (D1) and full (D2) pores in T and T-NT, respectively. E) High magnification images showing a cell cultured on the template T, which has empty pores (E1) and a cell cultured on the nano-structured template T-NT (E2), which has flexible nanotubes protruding from the pores (tubes stick because of the sample dehydration, see inset).

The nano-scaffold delays G1/S phase transition

As the increase of cell adhesion to the substrate is generally associated to the increase of cell proliferation, we investigated cell cycle progression. Surprisingly, we found a strong decrease of the number of DNA synthesizing cells (identified by EdU staining) on T-NT substrate with respect to the control T. Figure 2A plots the results of the continuous EdU labelling experiment, which is used as a method for cycle length evaluation [23].

When an asynchronous culture is incubated with EdU over the time, the y(0) intercept should give all the S phase cells labelled at the point of EdU addition, followed by a straight rise to the plateau value, which represents the percentage of cell cycling in the culture. More specifically, we found a linear increase of the percentage of DNA synthesizing cells over the time (the slope of the linear regression line is 0.013, R^2 = 0.91 for T group and 0.017, R^2 = 0.94 for the T-NT group), suggesting that there is a uniform cell population with a single cycle kinetics. Cells reach a similar plateau of 89.6%±2.8% and 88.5%±7.7% for T and T-NT, respectively (i.e. ~10% of cells do not cycle). However, cells reach the plateaux at very different time points, i.e. at 22.5 h and 38.2 h for T and T-NT, respectively. The interval from the start of the experiment to the point of plateaux represents the length of G2+M+G1 phases. We also found that there is no statistically significant difference in the duration of the M phase among groups (Figure 2B), being the M phase duration 2.10±0.17 h and 2.14±0.20 h for T and T-NT groups, respectively). Considering that G2 phase duration in NIH-3T3 cells is less than 1 h [23] and neglecting any change in G2 phase duration, we can assume that the nano-topography almost doubles G1 phase duration, with a delay in G1/S transition. The delay in G1/S phase transition is also confirmed by the expression level of cyclin E, which is essential for progression through the G1-phase of the cell cycle. In line with previous observations, we found a strong decrease of gene expression of cyclin E in T-NT treatment compared with T (p=0.0012). Altogether, these findings suggest that the nano-topography impairs progression from G1 phase to S phase, despite strongly enhanced cell adhesion.
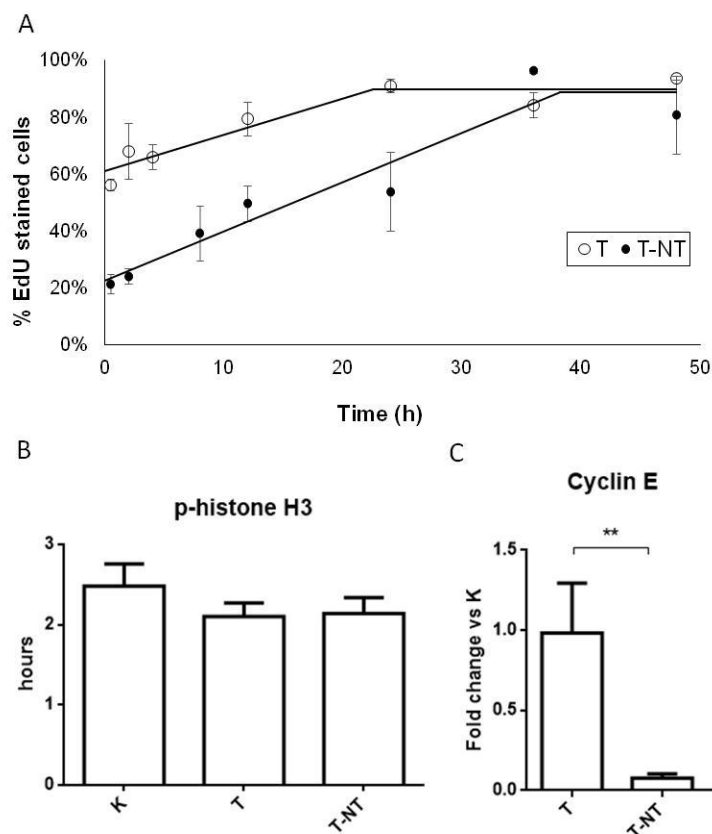
Figure 2. NIH-3T3 cells cultured on PLL-coated T, T-NT and K. A) EdU incubation at different time points. EdU is added at time point 0. N=3. Linear regression analysis, R² = 0.91 for T group and R² = 0.94 for the T-NT group. B) Duration of M phase by p-histone H3. N=6, one-way ANOVA, p=0.4. C) Cyclin E gene expression level comparison by Real-Time PCR. GAPDH gene used as internal control. ΔΔCt analysis performed against K. N=4, t-test, p=0.0012.

Interestingly, after 48 or 72h of continuous incubation on the substrates, we found that the percentage of necrotic cells or pyknotic nuclei was below 4% and 2%, respectively, for all groups (Figure S1, p>0.05). Cells cultured on the T-NT were also tested for longer incubation time (1 week): the number of necrotic cells and pyknotic nuclei was found to be 7.1±0.8% and 1.8±0.9%, respectively (n=3), suggesting that the delay of cell cycle progression is not the cause nor the consequence of any potential toxic effect triggered by nano-structured surface.

*Cell cycle progression is not dysregulated at adhesion point formation*

The first step of the adhesive process is adhesion assembly. During the formation of nascent adhesions, the actin filament cytoskeleton is coupled to the ECM via molecular clutches, i.e. transmembrane proteins such as integrins and cadherins. ECM triggers talin-dependent integrin activation, leading to the recruitment of scaffold proteins which link the clutch to the actin network [24]. As point contact adhesions appear to require integrin engagement, we compared the response of cells cultured on the substrates coated with poly-L-lysine, which does not bind integrins, and fibronectin, which does with high affinity. In line with previous observations, we found a strong decrease in the number of EdU positive cells on T-NT substrate with respect to the T and K control groups (Figure 3A, p<0.001), while the template T and K were not statistically different from each other (p>0.05). Interestingly, experimental results showed that there is no difference between the two coatings, for neither the nanostructured substrate T-NT nor the template T or the control plastic K (Figure 3A, p>0.05).
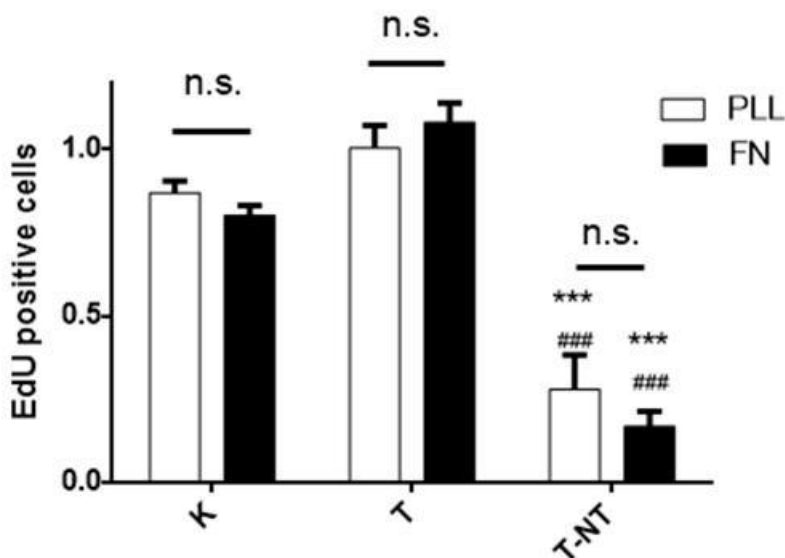
Figure 3. Fraction of EdU positive cells (incubation time 8h) with respect to the control K. N=6. 2-way ANOVA. * is the significance vs. the k group, # is the significance vs. the T group.

These results were confirmed by cytofluorimetry. Again, the percentage of EdU positive cells was almost halved in T-NT group with respect to T and K groups, with no difference between PLL and FN coatings (Figure 4). Cytotoxicity was also tested on FN-coated substrates, by confirming that the level of necrotic cells and pyknotic nuclei of cells grown on T-NT was not statistically different from control groups T and K, following 48 and 72h of continuous incubation (Figure S2).
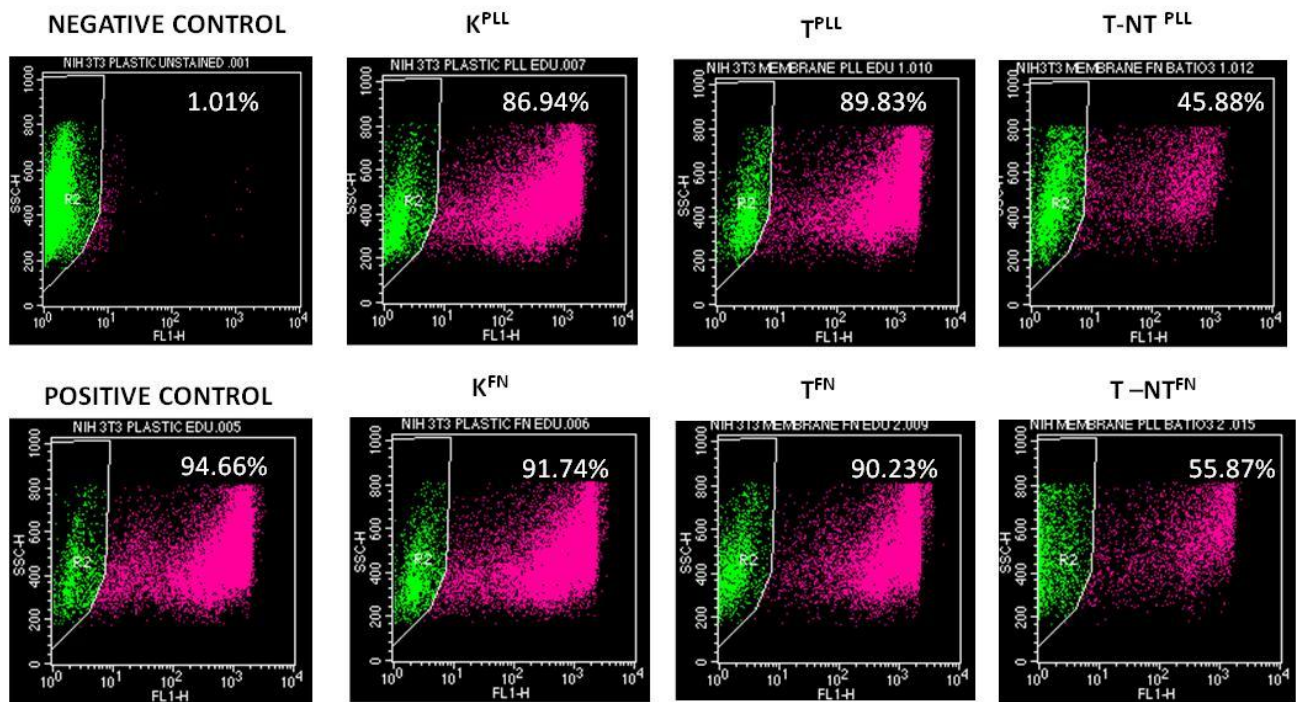
Figure 4. Cytofluorimetry of NIH-3T3 cells incubated with EdU for 18h. Percentage of EdU positive cells incubated on plastic (K), T, T-NT, coated with PLL or FN. The negative control is cells not stained with EdU. The positive control is cells cultured on uncoated plastic (K).

14

The formation of nascent point adhesions is not only responsible for the contact between cells and the ECM, but it also generates signals that remodel the cytoskeleton. In this context, an important scaffold MS protein is FAK, which is known to link cell adhesion to cell proliferation by the Ras-MAPK pathway via growth factor receptor-bound protein 2 (Grb2) or by FAK-dependent activation of ERK1/2 [25]. In order to explore the involvement of FAK, we used Tet-FAK inducible murine embryonic fibroblast (MEF) cells derived from FAK-deficient mice [21]. We tested two different clones of inducible Tet-FAK cells expressing FAK: one harbouring wild type FAK and the other, mutated FAK(F397) [26]. FAK(F397) is mutated at tyrosine residue 397, the integrin-stimulated phosphorylation of which creates a high-affinity site that is recognized by several SH2 domain-containing proteins. As expected, in MEF expressing FAK, the percentage of DNA synthesizing cells strongly decreases when cells are cultured on the nanostructured substrate T-NT compared to the template T (Figure 5), with the same values found for NIH-3T3 (Figure 2A, time point 8 h). However, we found no statistical difference when cells do not express FAK or express the mutated variant, excluding involvement of FAK in the delay of G1/S phase transition.
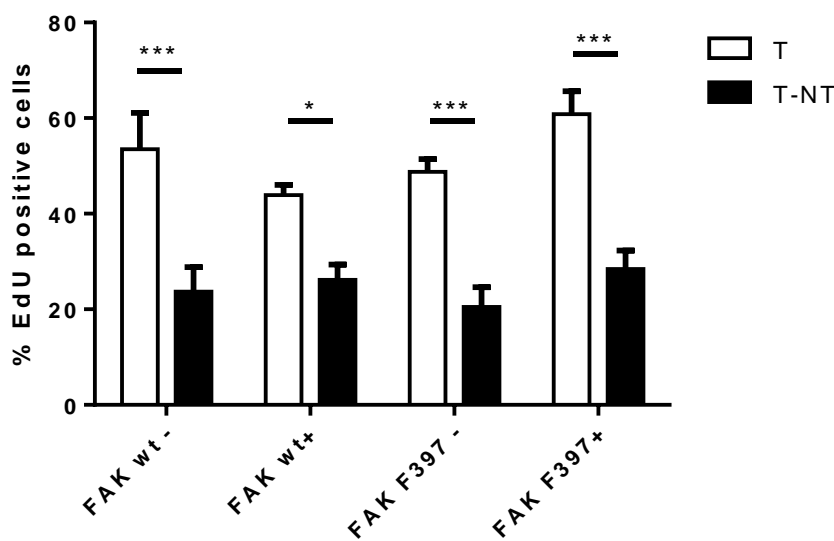
Figure 5. MEF cells incubated with EdU for 8h on FN-coated T and T-NT. N=6. 2-way ANOVA, row factor p=0.11, column factor p<0.0001.

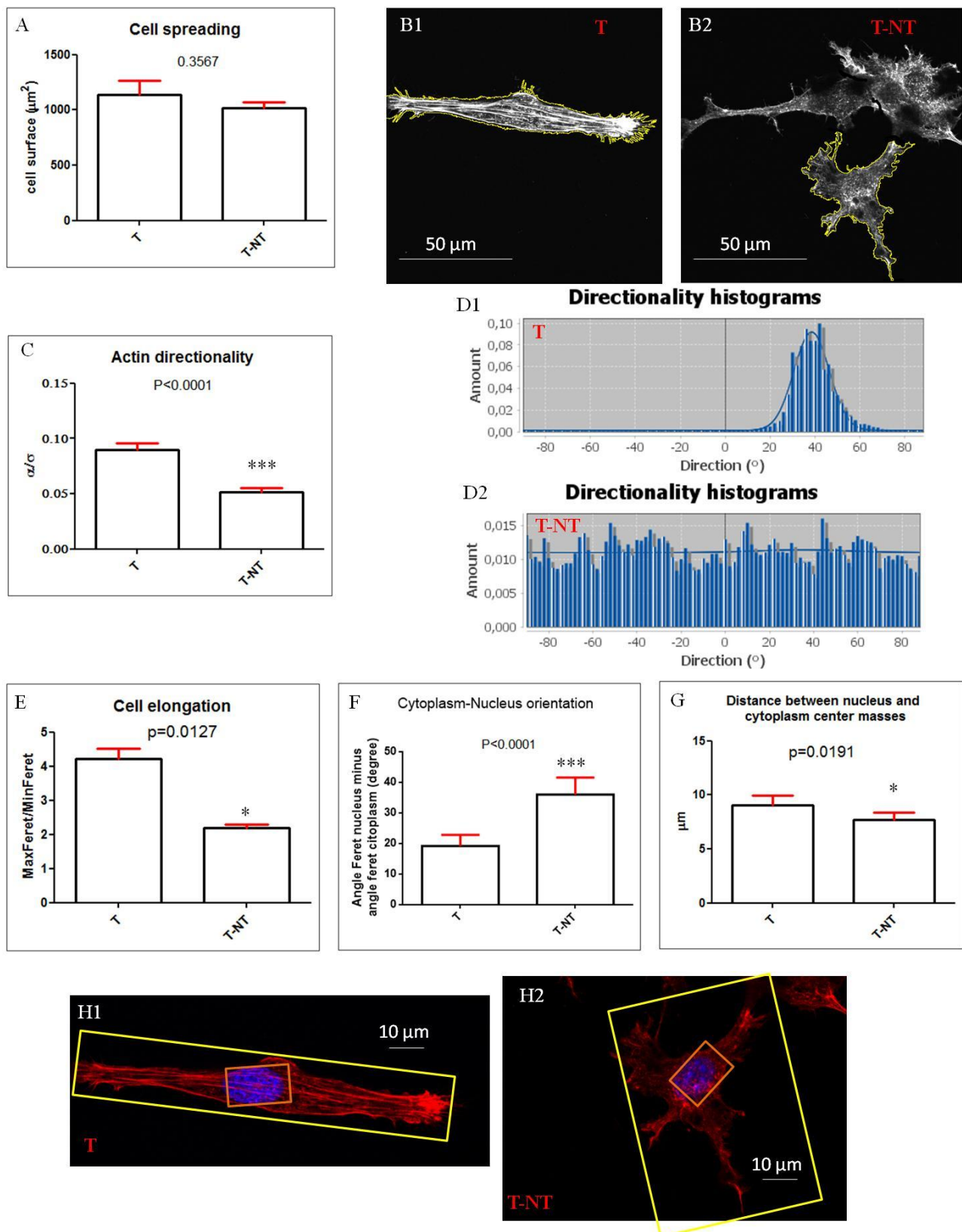*Nano-topography impairs the formation of stress fibers*

The 5-fold increase of area exposed by the nano-structured surface provides increased concentration of adhesion molecules, which accounts for the excellent cell spreading and the enhanced adhesion we observed on the T-NT substrates (Figure 1, Figure 6). However, our results suggest cells grown on nano-topography are unable to produce stress fibers. Figure 6 shows the typical organization of actin cytoskeleton in cells grown on T and T-NT substrate. Cells grown on the template T show dorsal stress fibers and the typical ventral fibers, which span from the adhesion point close to the cell edge to an adhesion site near the nucleus [27]. These stress fibers are almost absent in cells grown on T-NT. Here, actin filaments are highly concentrated at the periphery of the cell, where the plasma membrane anchors the nano-topography. These peripheral attachments of actin filaments are particularly evident in fibroblasts cultured on T-NT compared to the fibroblast cultured on T. As a consequence of this different organization of actin stress fiber, cells cultured on T and T-NT exhibit a very different morphology. Fibroblasts grown on the control template T have ventral and dorsal stress fiber, which are the transmitters of contractile force to the entire actin cytoskeleton, thus being highly polarized. In contrast, in fibroblasts grown on T-NT, stress fibers are not cytoplasmic but are mainly associated with the plasma membrane anchoring the nano-topography, resulting in non-polarized cells with numerous randomly oriented protrusions of the cell membrane.
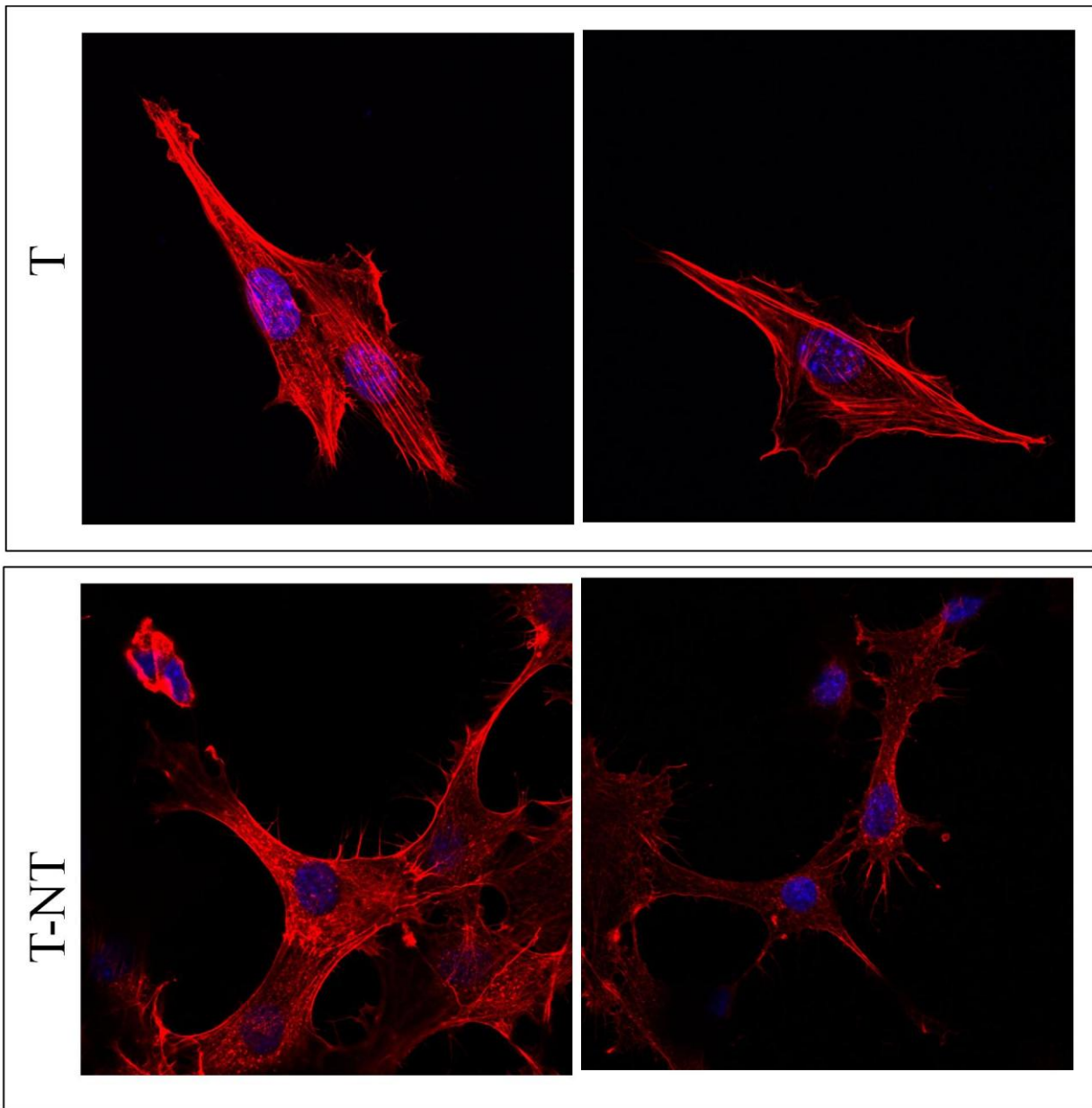
16

Figure 6. Cells grown on T or T-NT substrates: actin staining (red) and nuclear staining (blue). The image size is 123 μm x 123 μm.

These qualitative observations are fully supported by quantitative analysis. By examining a random population of 65 cells from 3 independent biological assays, we collected and plotted data on cell morphology and organization of actin bundles. Although cell spreading is similar between the two groups (the surface area of cells grown on T and T-NT substrates was similar, Figure 7A, p=0.36), the organization of actin cytoskeleton was completely different. By analyzing the direction of actin bundles, we found that cells

cultured on T, actin exhibited a preferential orientation, corresponding to the peak of the Gaussian function of the directionality histogram (Figure 7D1). In contrast, in cells cultured on T-NT, there is no preferential actin orientation and the directionality histogram appears to be flat (Figure 7D2), indicating that actin bundles are randomly orientated. For each cell, we calculated the ratio α/σ, where σ is standard deviation of the Gaussian and α is the sum of the histogram from center- σ to center+ σ. Narrow Gaussian distributions have low ratio values, while tall Gaussian distributions have high ratio values. In agreement with the observation that cells cultured on T-NT do not have cytoplasmic stress fibers, we found that the ratio α/σ is halved in cells grown on T-NT compared to cells grown on T (p=0.0015). Quantitative data also confirm that, as consequence of the absence of cytosplasmic stress fibers, cells cultured on T-NT lose their polarity. In fact, the cell elongation characteristic of fibroblasts is strongly reduced and the elongation factors were halved (from 4.2±0.3 for T group to 2.2±0.1 for T-NT group, p=0.0127). Similarly, in the well-polarized cells cultured on T, cell cytoplasm and nucleus tends to be aligned in the same direction, while in cells cultured on T-NT the relative orientation between cell nucleus and cytoplasm is random (Figure 7F). We analyzed also the distance between the centers of mass of cell and nucleus, in line with previous observation; we found this distance decreases in less polarized cells grown on T-NT compared to the highly polarized cells grown on T (Figure 7G, p=0.0191).

Figure 7. A) Cell surface area (μm^2). The groups T and T-NT are not statistically different (t-test, p=0.3567). For each cell, cell surface was given as area of the ROI corresponding to the cell boundary (e.g., yellow line in B1-2). B1) and B2) are examples of cell boundary calculation from the images of phalloidin staining for the T group and T-NT group,

respectively. C) Cells grown on T have an actin network which exhibits a preferential orientation, while cells grown on T-NT are less oriented (t-test, p=0.0015). Actin directionality was calculated from actin directionality histograms. D) The actin directionality histograms indicate the amount of actin staining in a given direction. Cells in which there is a preferred orientation of actin are expected to give a histogram with a peak at that orientation as depicted in panel D1), which is the histogram of the cell (yellow shaped) grown on T of panel B1. Cells with completely isotropic actin content are expected to give a flat histogram, as depicted in panel D2), which is the histogram of the cell (yellow shaped) grown on T-NT of panel B2. E) Cells grown on T-NT are less elongated compared to the control cells (t-test, p=0.0127). The elongation is expressed as ratio between the maxFeret and the minFeret. F) In cells grown on T, the cytoplasm and the nucleus have a similar orientation, while in cells grown on T-NT, their respective orientation appears to be random (t-test, p<0.0001). Data provided denote difference between the angle Feret of the cytoplasm and the angle Feret of the nucleus (absolute value). G) In cells grown on T-NT the nucleus is preferentially localized in the center of the cytoplasm, while cells grown on T exhibits a higher polarity (t-test, p=0.0191). Data provided denote distance between the centers of mass of cytoplasm and nucleus. H) The maxFeret and the minFeret are approximately the big and the small sides of the parallelogram in the panels. The representation of maxFeret and minFeret of cytoplasm (yellow parallelogram) and nucleus (orange parallelogram) for the cell of panel B1 and for the cell of panel B2 are shown in H1) and H2), respectively. N=65.
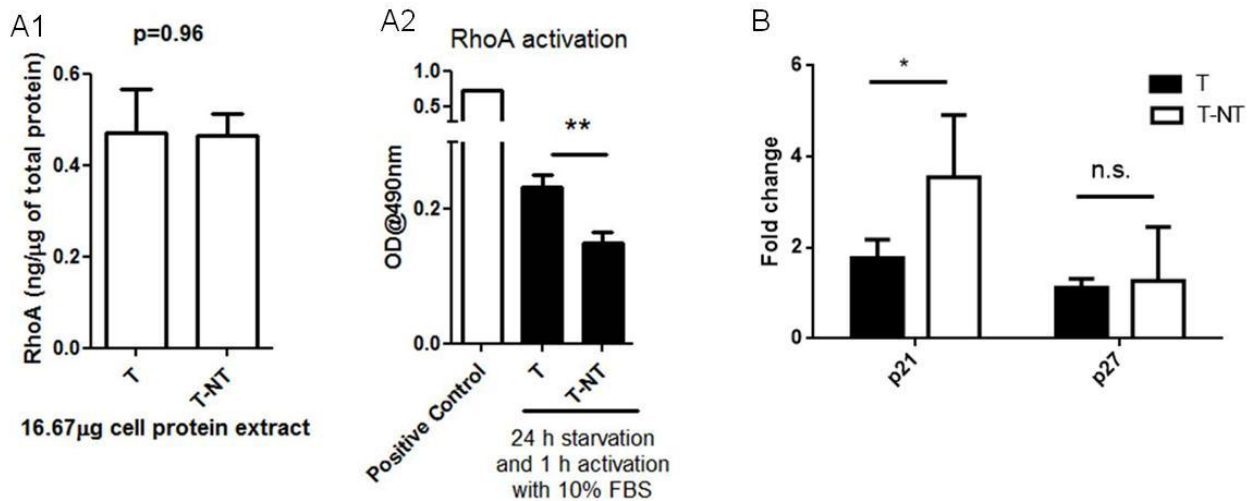
The delay of G1/S transition is mediated by RhoA and p21

In view of the absence on cytosolic stress fibers in cells cultured on nano-structured surfaces, we focused our attention on the small GTPase RhoA, which is a key regulator of stress fiber formation [28]. Rho is activated in response to mechanical strain.

20

Increased activation level of Rho kinase ultimately leads to an increased level of phosphorylation of the regulatory subunit of myosin II and its association with actin filaments. Myosin II crosslinks actin filaments to create stress fibers and generates tension on actin filaments, thereby promoting changes in the cytoskeleton necessary to withstand force. Our experimental results indicated that although total RhoA level is similar between the T and T-NT conditions (Figure 8A1, p=0.96), the level of active RhoA is substantially lower in cells cultured on nano- structured surfaces with respect to the control template (Figure 8A2, p= 0.0068). This suggests that fibroblasts cultured on nano-structured surfaces are unable to develop the mechanical strain required for RhoA activation. Interestingly, it has been demonstrated in NIH-3T3 cells that when RhoA signaling is inhibited, Ras up-regulates the expression of the cyclin-dependent-kinase inhibitor p21Waf1/Cip1, which associates with and inhibits cyclin E-CDK2 activity, blocking the entry into the S phase of the cell cycle [29]. This regulation occurs through a transcriptional mechanism, which is independent of p53 [30]. RhoA also regulates p27kip21 but the mechanism is not transcriptional and is associated with mitogen-induced p27 degradation [31]. We compared expression levels of p21 and p27 between T and T-NT conditions. As expected, we observed an increase of p21 expression level (Figure 8B, p=0.0465) in cells cultured on nano-topography, while p27 expression was not significantly different (Figure 8B, p=0.75).

21

Figure 8. A) Level of total and active RhoA. A1) The amount of total RhoA was quantified by the calibration curve abs=0.078x, R²=0.9, obtained with known amount of RhoA (1.1, 3.3, 10 and 30ng). There is no difference in total RhoA between T and T-NT groups. n=5, t-test, p=0.96. A2) The positive control (K+) is RhoA constitutively active. T and T-NT groups are significantly different. N=5, t-test, p=0.0068. B) Gene expression level of p21 and p27: comparison between T and T-NT. The internal control is the GAPDH gene. ΔΔCt analysis was performed against normal plastic control. N=4, t-test, p=0.046 and p=0.75 for p21 and p27, respectively.

Discussion

Proper cell spreading is considered a general requirement for high RhoA/ROCK activity and stress fiber formation, while cells with small, rounded shapes are generally associated with low RhoA/ROCK activity [32]. In this work, we used nanotechnology to decouple cell spreading from stress fiber formation. Specifically, we artificially created a microenvironment, which strongly promotes cell adhesion but inhibit stress fiber formation. In fact, the increase of available surface area increases the density of adhesion molecules, resulting in high cell spreading (Figure 7), intimate contact with the matrix (Figure 1C) and enhanced matrix attachments compared to controls. However, the mechanical behaviour of nano-topography is like quicksand, and tightly envelops point

adhesions, thereby undermining the cell efforts to push against the matrix. Obviously, this influences cell signaling. Activation of RhoA is inhibited (Figure 8), as the ability to develop stress fibers (Figure 6, 7). Consequently, we observed that the duration of G1 phase is almost doubled with respect to the controls (Figure 2, 3, 4) because the activation of RhoA is required to remove the inhibition actuated by p21/p27 needed for G1 to S phase transition [29]. Our experimental results suggest that acto-myosin contraction is tightly coupled with cell proliferation, which decreases when acto-myosin contraction is impaired, even in presence of strong cell adhesion. In fact, several lines of evidence such as the enhanced cell adhesion to the nano-topography, the excellent cell spreading (Figure 7), the non-involvement of coating type (Figure 3-4) and FAK signaling (Figure 5), suggest that although the adhesion process proceeds, it does not account for the increased duration of the G1 phase. The lack of stress fibers suggests that nano-topography stops the transmission of out-to-inside force from adhesion points to actin cytoskeleton and, consequently, the achievement of the critical tensional homeostasis, which is required for RhoA activation and RhoA-dependent suppression of p21 levels (Figure 8).

Although nano-topography provides an artificial environment, it could, at least in principle, be akin to the *in vivo* situation exemplified by the role of the ECM. In fact, it is generally recognized that the stiffness and nanometer-size characteristics of the ECM influences numerous physiological and pathological processes *in vivo* [33]. The ECM provides multiple cues to the cells, such as pore size, stiffness, nano-topography and dimensionality, which are totally lacking in *in vitro* cell cultures. Additionally, the nano-topographical cues and the compliance of ECM are continuously remodeled *in vivo* during normal development and in diseased tissues [34]. In this context, one could argue that, similar to nano-topography, ECM cell proliferation could be altered by direct

23

modulation of acto-myosin contractility, without necessarily influencing the adhesive process or changes in cell shape.

Reference

[1] Yusko EC, Asbury CL. Force is a signal that cells cannot ignore. Molecular biology of the cell. 2014;25:3717-25.

[2] Wozniak MA, Chen CS. Mechanotransduction in development: a growing role for contractility. Nature reviews Molecular cell biology. 2009;10:34-43.

[3] Bellas E, Chen CS. Forms, forces, and stem cell fate. Current opinion in cell biology. 2014;31:92-7.

[4] Lo CM, Wang HB, Dembo M, Wang YL. Cell movement is guided by the rigidity of the substrate. Biophysical journal. 2000;79:144-52.

[5] Provenzano PP, Keely PJ. Mechanical signaling through the cytoskeleton regulates cell proliferation by coordinated focal adhesion and Rho GTPase signaling. Journal of cell science. 2011;124:1195-205.

[6] Seong J, Wang N, Wang Y. Mechanotransduction at focal adhesions: from physiology to cancer development. Journal of cellular and molecular medicine. 2013;17:597-604.

[7] Geiger B, Spatz JP, Bershadsky AD. Environmental sensing through focal adhesions. Nature reviews Molecular cell biology. 2009;10:21-33.

[8] Wang N, Tytell JD, Ingber DE. Mechanotransduction at a distance: mechanically coupling the extracellular matrix with the nucleus. Nature reviews Molecular cell biology. 2009;10:75-82.

[9] Graham DM, Burridge K. Mechanotransduction and nuclear function. Current opinion in cell biology. 2016;40:98-105.

24

[10] Parsons JT, Horwitz AR, Schwartz MA. Cell adhesion: integrating cytoskeletal dynamics and cellular tension. Nature reviews Molecular cell biology. 2010;11:633-43.

[11] Nobes CD, Hall A. Rho, rac, and cdc42 GTPases regulate the assembly of multimolecular focal complexes associated with actin stress fibers, lamellipodia, and filopodia. Cell. 1995;81:53-62.

[12] Myers JP, Robles E, Ducharme-Smith A, Gomez TM. Focal adhesion kinase modulates Cdc42 activity downstream of positive and negative axon guidance cues. Journal of cell science. 2012;125:2918-29.

[13] Price LS, Leng J, Schwartz MA, Bokoch GM. Activation of Rac and Cdc42 by integrins mediates cell spreading. Molecular biology of the cell. 1998;9:1863-71.

[14] Hoon JL, Tan MH, Koh CG. The Regulation of Cellular Responses to Mechanical Cues by Rho GTPases. Cells. 2016;5.

[15] Provenzano PP, Inman DR, Eliceiri KW, Keely PJ. Matrix density-induced mechanoregulation of breast cell phenotype, signaling and gene expression through a FAK-ERK linkage. Oncogene. 2009;28:4326-43.

[16] Assoian RK, Klein EA. Growth control by intracellular tension and extracellular stiffness. Trends in cell biology. 2008;18:347-52.

[17] Mih JD, Marinkovic A, Liu F, Sharif AS, Tschumperlin DJ. Matrix stiffness reverses the effect of actomyosin tension on cell proliferation. Journal of cell science. 2012;125:5974-83.

[18] Walker JL, Fournier AK, Assoian RK. Regulation of growth factor signaling and cell cycle progression by cell adhesion and adhesion-dependent changes in cellular tension. Cytokine & growth factor reviews. 2005;16:395-405.

[19] Giannini M, Giannaccini M, Sibillano T, Giannini C, Liu D, Wang Z, et al. Sheets of vertically aligned BaTiO3 nanotubes reduce cell proliferation but not viability of NIH-3T3 cells. PloS one. 2014;9:e115183.

25

[20] Chen YY, Yu BY, Wang JH, Cochran RE, Shyue JJ. Template-Based Fabrication of SrTiO3 and BaTiO3 Nanotube. Inorganic Chemistry. 2009;48:681-6.

[21] Owen JD, Ruest PJ, Fry DW, Hanks SK. Induced focal adhesion kinase (FAK) expression in FAK-null cells enhances cell spreading and migration requiring both auto- and activation loop phosphorylation sites and inhibits adhesion-dependent tyrosine phosphorylation of Pyk2. Molecular and cellular biology. 1999;19:4806-18.

[22] Baxter FR, Bowen CR, Turner IG, Dent AC. Electrically active bioceramics: a review of interfacial responses. Ann Biomed Eng. 2010;38:2079-92.

[23] Schorl C, Sedivy JM. Analysis of cell cycle phases and progression in cultured mammalian cells. Methods. 2007;41:143-50.

[24] DeMali KA, Sun XW, Bui GA. Force Transmission at Cell-Cell and Cell-Matrix Adhesions. Biochemistry-Us. 2014;53:7706-17.

[25] Zhao JH, Reiske H, Guan JL. Regulation of the cell cycle by focal adhesion kinase. The Journal of cell biology. 1998;143:1997-2008.

[26] Ilic D, Furuta Y, Kanazawa S, Takeda N, Sobue K, Nakatsuji N, et al. Reduced cell motility and enhanced focal adhesion contact formation in cells from FAK-deficient mice. Nature. 1995;377:539-44.

[27] Small JV, Rottner K, Kaverina I, Anderson KI. Assembling an actin cytoskeleton for cell attachment and movement. Biochimica et biophysica acta. 1998;1404:271-81.

[28] Chrzanowska-Wodnicka M, Burridge K. Rho-stimulated contractility drives the formation of stress fibers and focal adhesions. The Journal of cell biology. 1996;133:1403-15.

[29] Olson MF, Paterson HF, Marshall CJ. Signals from Ras and Rho GTPases interact to regulate expression of p21Waf1/Cip1. Nature. 1998;394:295-9.

[30] Vogt A, Sun J, Qian Y, Hamilton AD, Sebti SM. The geranylgeranyltransferase-I inhibitor GGTI-298 arrests human tumor cells in G0/G1 and induces

p21(WAF1/CIP1/SDI1) in a p53-independent manner. The Journal of biological chemistry. 1997;272:27224-9.

[31] Jakel H, Peschel I, Kunze C, Weinl C, Hengst L. Regulation of p27 (Kip1) by mitogen-induced tyrosine phosphorylation. Cell cycle. 2012;11:1910-7.

[32] McBeath R, Pirone DM, Nelson CM, Bhadriraju K, Chen CS. Cell shape, cytoskeletal tension, and RhoA regulate stem cell lineage commitment. Developmental cell. 2004;6:483-95.

[33] Yang Y, Wang K, Gu X, Leong KW. Biophysical Regulation of Cell Behavior-Cross Talk between Substrate Stiffness and Nanotopography. Engineering. 2017;3:36-54.

[34] Bonnans C, Chou J, Werb Z. Remodelling the extracellular matrix in development and disease. Nature reviews Molecular cell biology. 2014;15:786-801.

Figure legends

Figure 1. A) AFM image of the flat template T. B) AFM image of the nano-structured template T-NT. C) Low magnification image showing a NIH-3T3 cell cultured on T-NT. D) SEM imaging of empty (D1) and full (D2) pores in T and T-NT, respectively. E) High magnification images showing a cell cultured on the template T, which has empty pores (E1) and a cell cultured on the nano-structured template T-NT (E2), which has flexible nanotubes protruding from the pores (tubes stick because of the sample dehydration, see inset).

Figure 2. NIH-3T3 cells cultured on PLL-coated T, T-NT and K. A) EdU incubation at different time points. EdU is added at time point 0. N=3. Linear regression analysis, $R^2 =$ 0.91 for T group and $R^2 = 0.94$ for the T-NT group. B) Duration of M phase by p-histone H3. N=6, one-way ANOVA, p=0.4. C) Cyclin E gene expression level comparison by Real-Time PCR. GAPDH gene used as internal control. ΔΔCt analysis performed against K. N=4, t-test, p=0.0012.

Figure 3. A) Fraction of EdU positive cells (incubation time 8h) with respect to the control K. N=6. 2-way ANOVA. * is the significance vs. the k group, # is the significance vs. the T group.

Figure 4. Cytofluorimetry of NIH-3T3 cells incubated with EdU for 18h. Percentage of EdU positive cells incubated on plastic (K), T, T-NT, coated with PLL or FN. The negative control is cells not stained with EdU. The positive control is cells cultured on uncoated plastic (K).

Figure 5. MEF cells incubated with EdU for 8h on FN-coated T and T-NT. N=6. 2-way ANOVA, row factor p=0.11, column factor p<0.0001.

Figure 6. Cells grown on T or T-NT substrates: actin staining (red) and nuclear staining (blue). The image size is 123 μm x 123 μm.

Figure 7. A) Cell surface area (μm2). The groups T and T-NT are not statistically different (t-test, p=0.3567). For each cell, cell surface was given as area of the ROI corresponding to the cell boundary (e.g., yellow line in B1-2). B1) and B2) are examples of cell boundary calculation from the images of phalloidin staining for the T group and T-NT group, respectively. C) Cells grown on T have an actin network which exhibits a preferential orientation, while cells grown on T-NT are less oriented (t-test, p=0.0015). Actin directionality was calculated from actin directionality histograms. D) The actin directionality histograms indicate the amount of actin staining in a given direction. Cells in which there is a preferred orientation of actin are expected to give a histogram with a peak at that orientation as depicted in panel D1), which is the histogram of the cell (yellow shaped) grown on T of panel B1. Cells with completely isotropic actin content are expected to give a flat histogram, as depicted in panel D2), which is the histogram of the cell (yellow shaped) grown on T-NT of panel B2. E) Cells grown on T-NT are less elongated compared to the control cells (t-test, p=0.0127). The elongation is expressed as ratio between the maxFeret and the minFeret. F) In cells grown on T, the cytoplasm and the nucleus have a similar orientation, while in cells grown on T-NT, their respective orientation appears to be random (t-test, p<0.0001). Data provided denote difference between the angle Feret of the cytoplasm and the angle Feret of the nucleus (absolute value). G) In cells grown on T-NT the nucleus is preferentially localized in the center of the cytoplasm, while cells grown on T exhibits a higher polarity (t-test, p=0.0191). Data provided denote distance between the centers of mass of cytoplasm and nucleus. H) The maxFeret and the minFeret are approximately the big and the small sides of the parallelogram in the panels. The representation of maxFeret and minFeret of cytoplasm

(yellow parallelogram) and nucleus (orange parallelogram) for the cell of panel B1 and for the cell of panel B2 are shown in H1) and H2), respectively. N=65.

Figure 8. A) Level of total and active RhoA. A1) The amount of total RhoA was quantified by the calibration curve abs=0.078x, R^2=0.9, obtained with known amount of RhoA (1.1, 3.3, 10 and 30ng). There is no difference in total RhoA between T and T-NT groups. n=5, t-test, p=0.96. A2) The positive control (K+) is RhoA constitutively active. T and T-NT groups are significantly different. N=5, t-test, p=0.0068. B) Gene expression level of p21 and p27: comparison between T and T-NT. The internal control is the GAPDH gene. ΔΔCt analysis was performed against normal plastic control. N=4, t-test, p=0.046 and p=0.75 for p21 and p27, respectively.

Figure1
Click here to download high resolution image
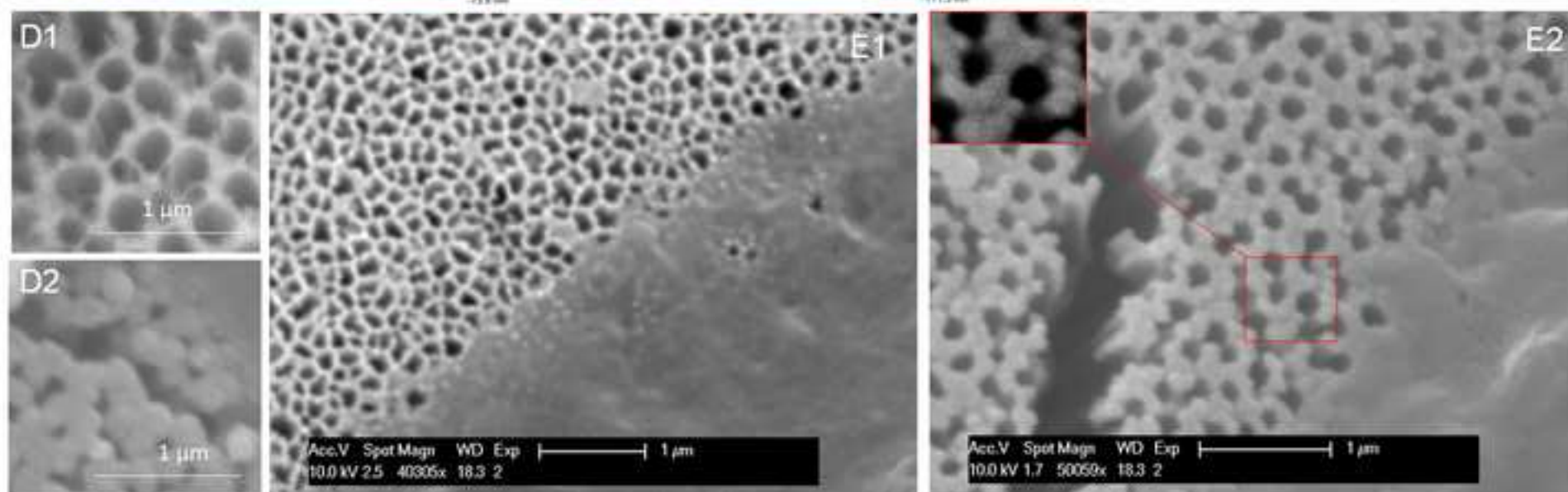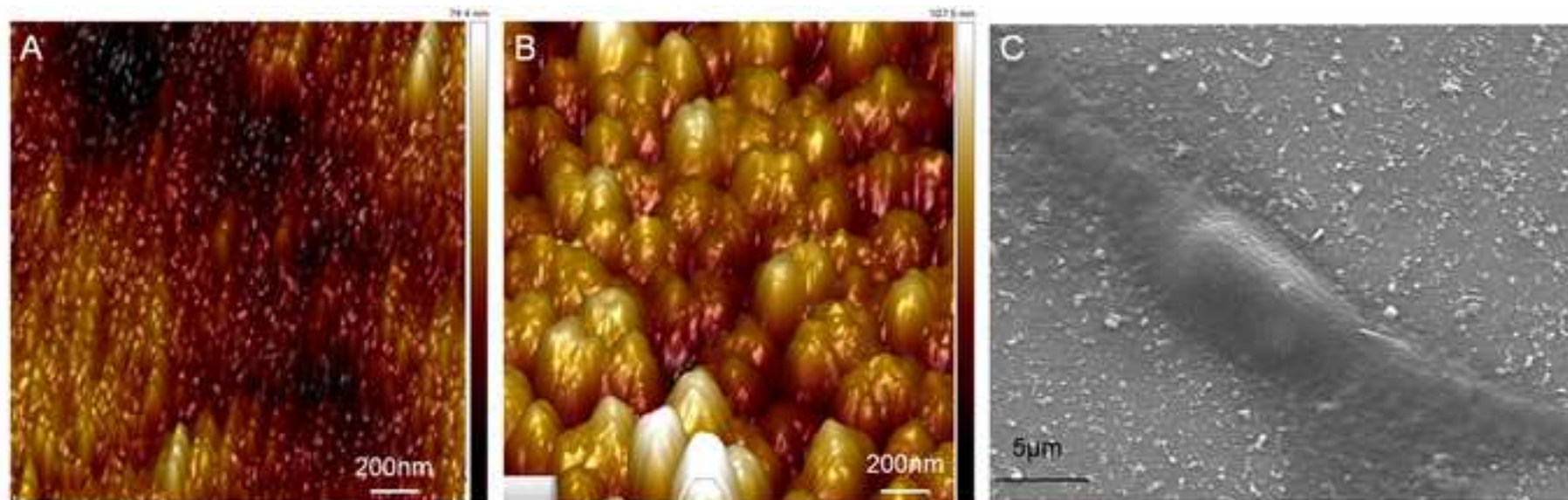
Figure2
Click here to download high resolution image
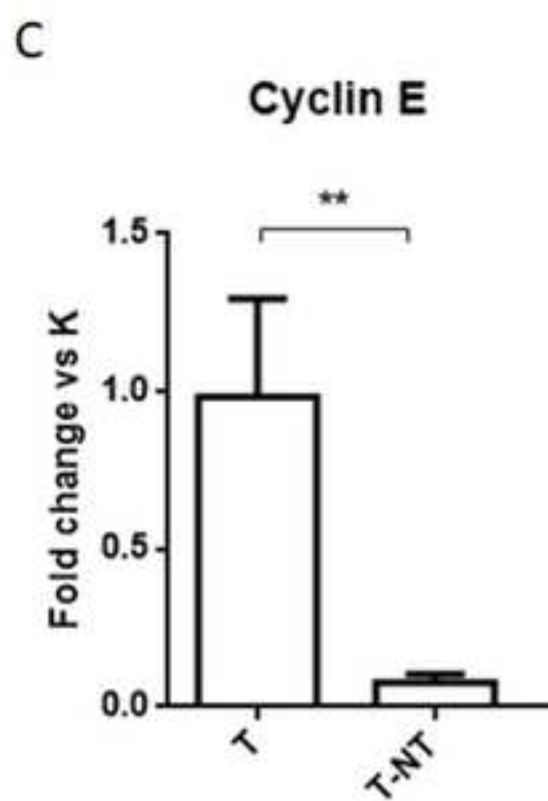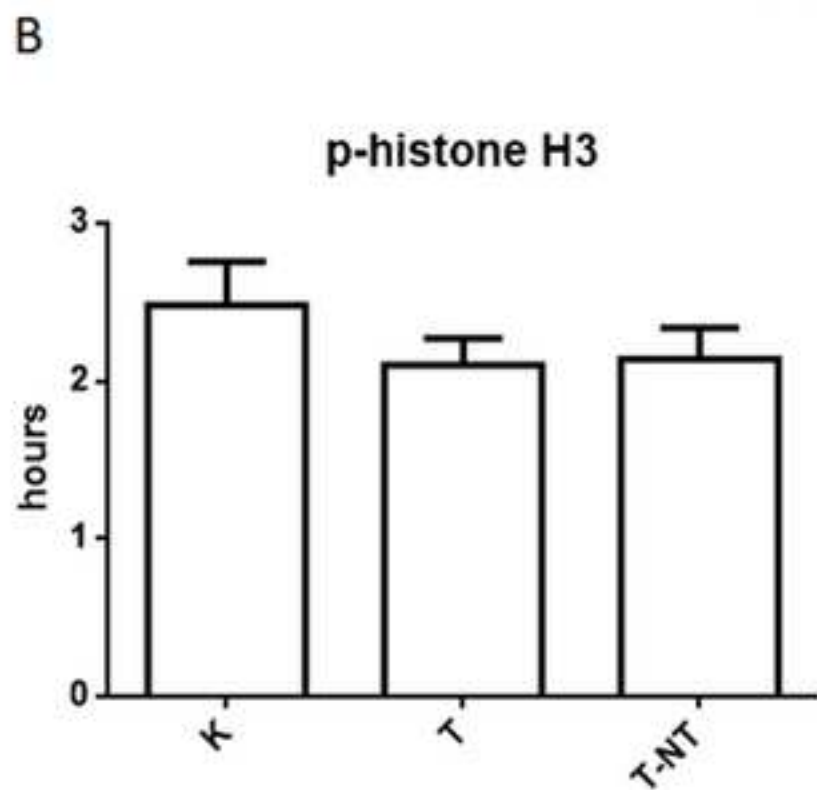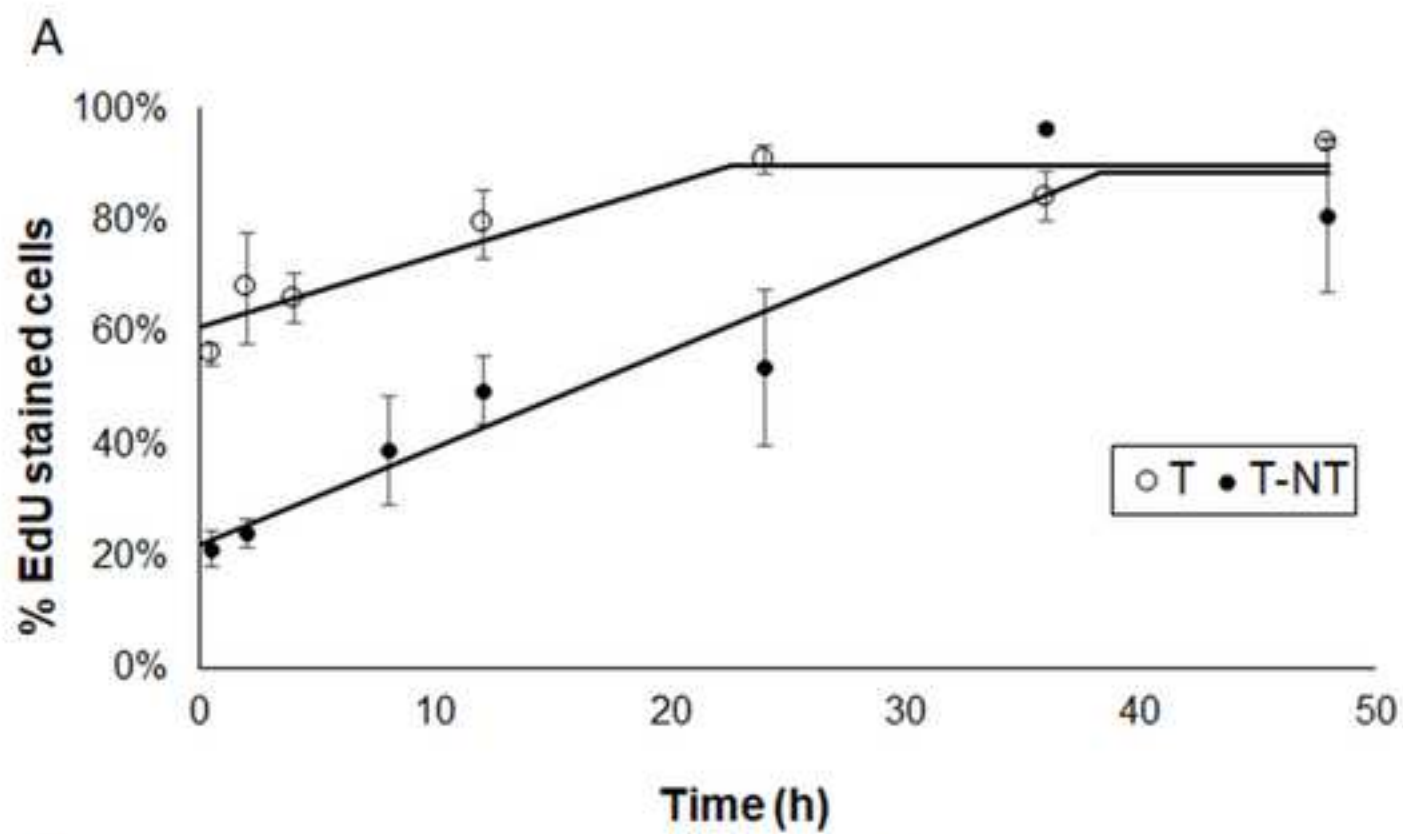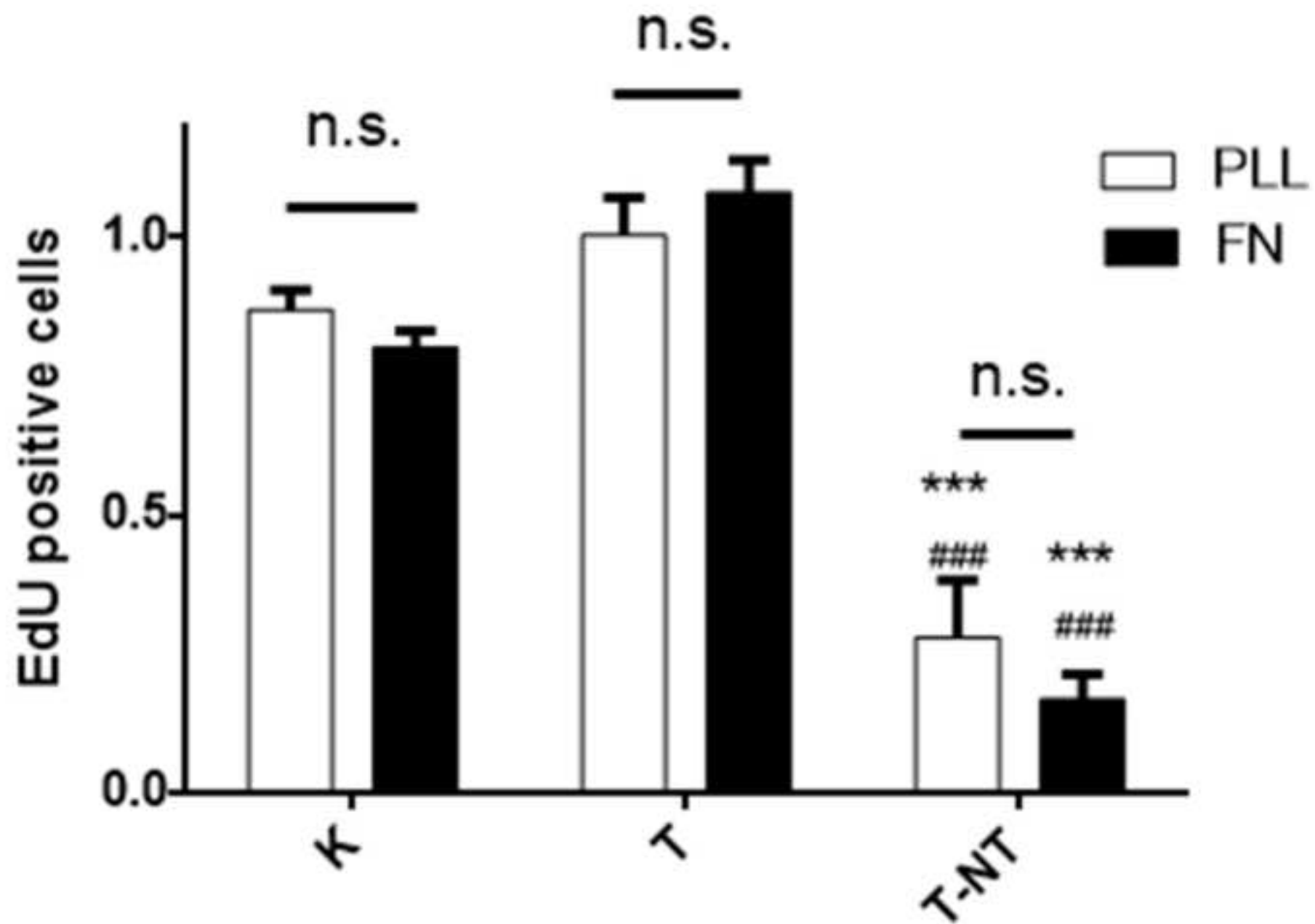
Figure4
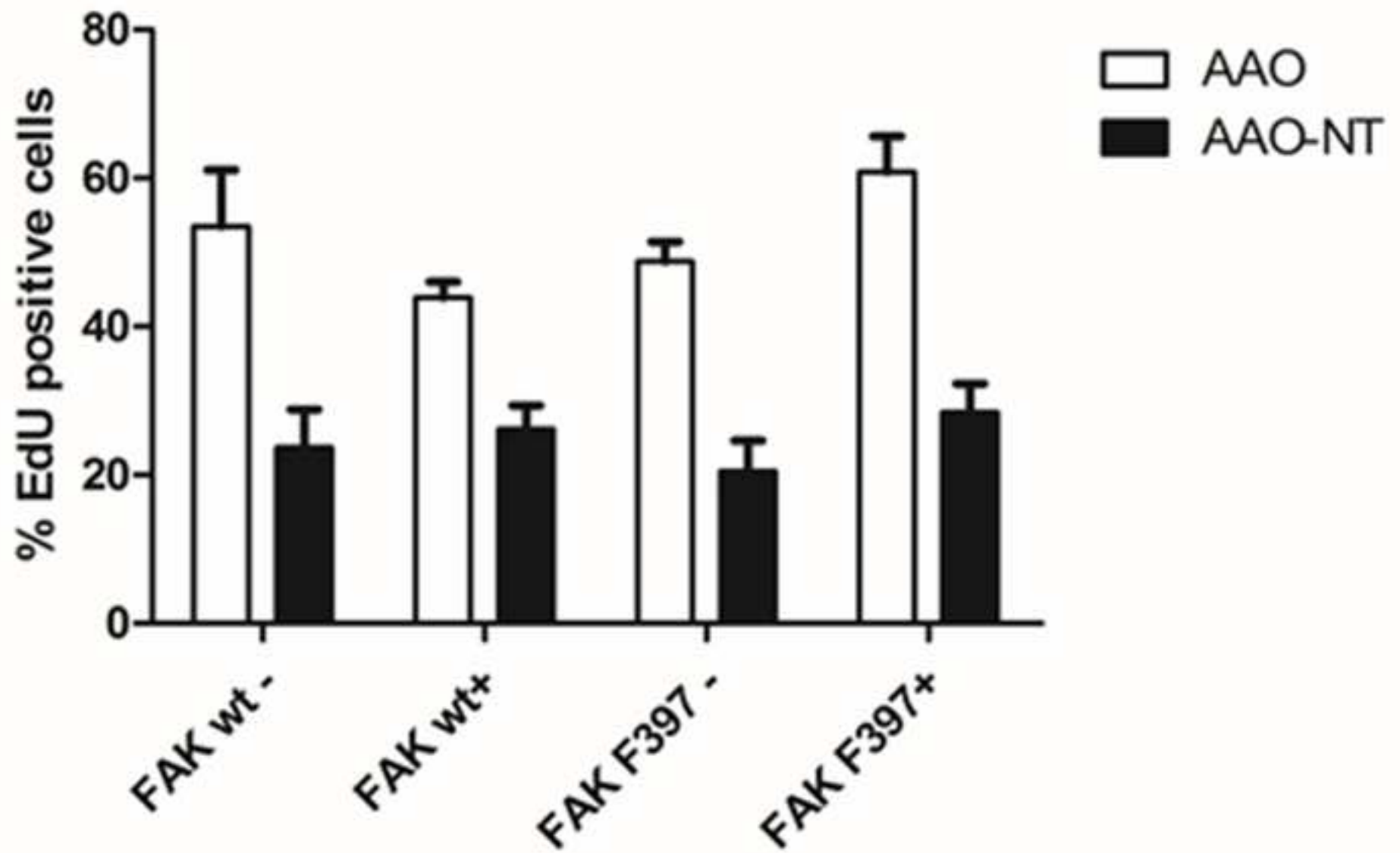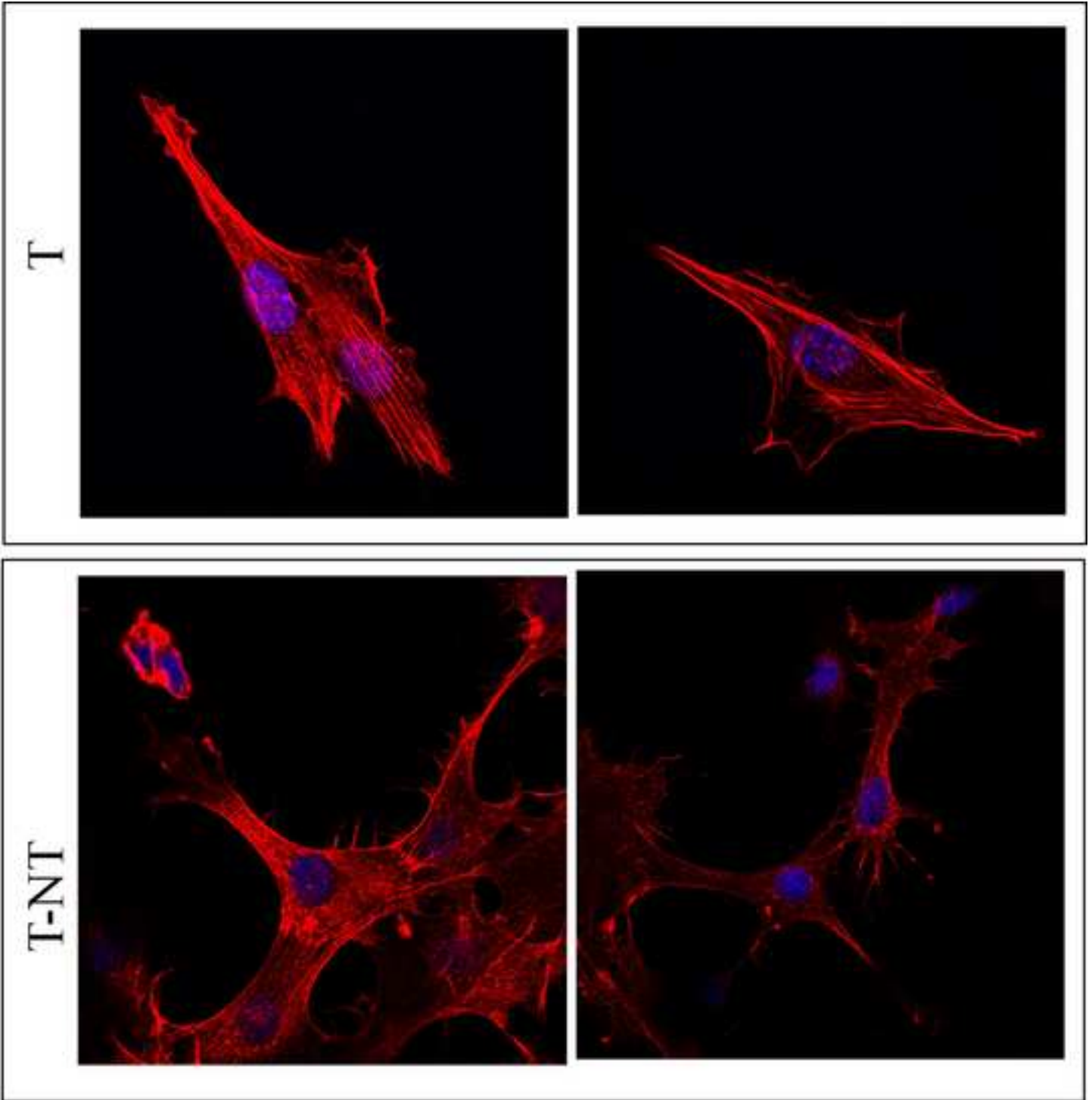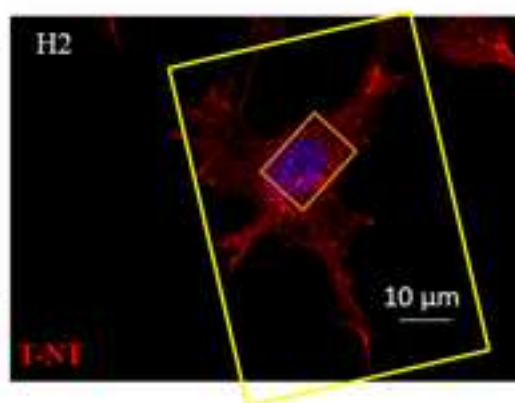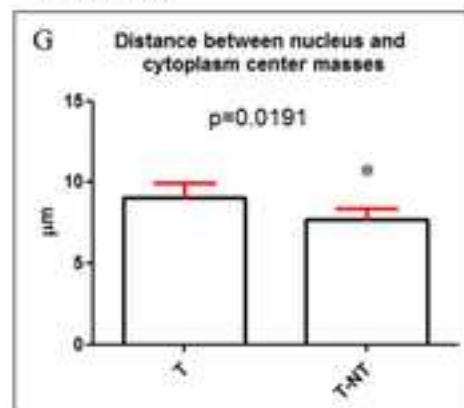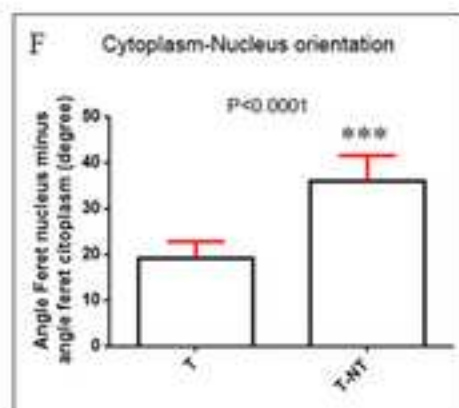**Click here to download high resolution image**

NEGATIVE CONTROL — 1.01%

K^{PLL} — 86.94%

T^{PLL} — 89.83%

T-NT^{PLL} — 45.88%

POSITIVE CONTROL — 94.66%

K^{FN} — 91.74%

T^{FN} — 90.23%

T–NT^{FN} — 55.87%
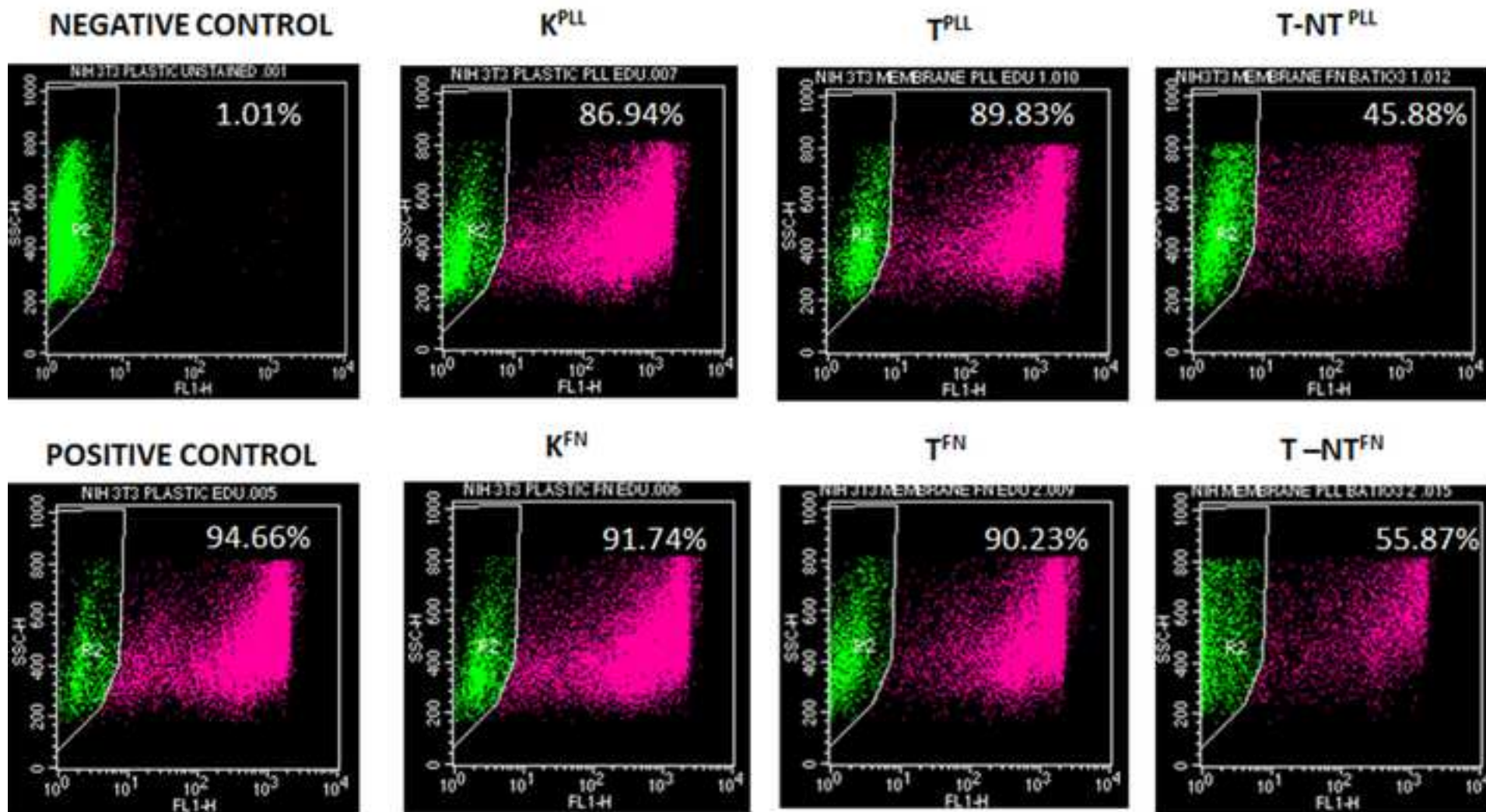
Figure6
Click here to download high resolution image

Figure7
Click here to download high resolution image
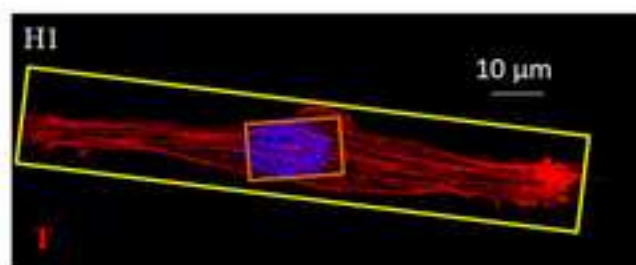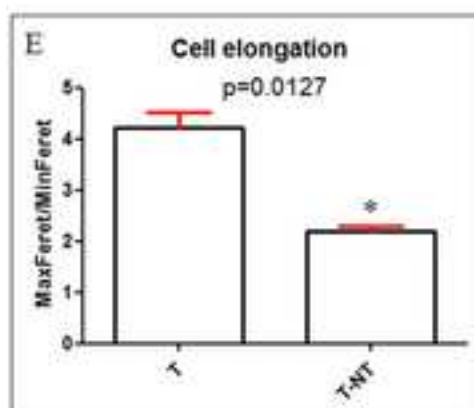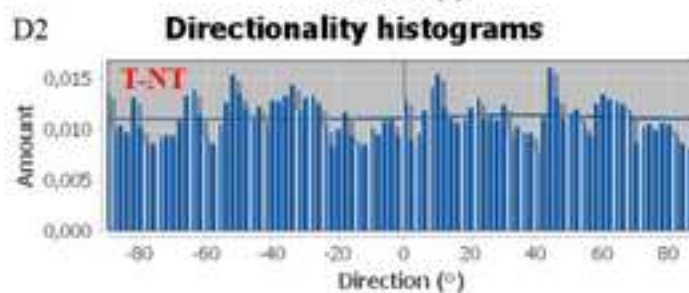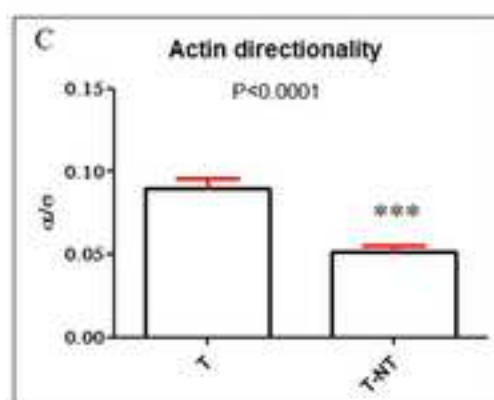
Figure8

Supplementary Material

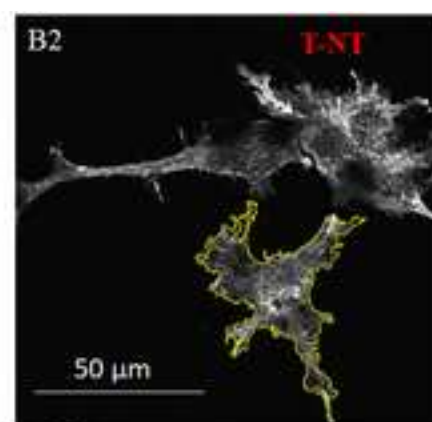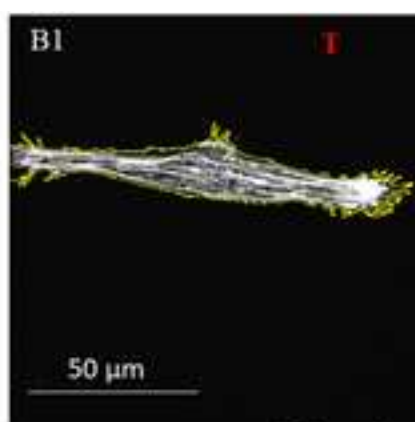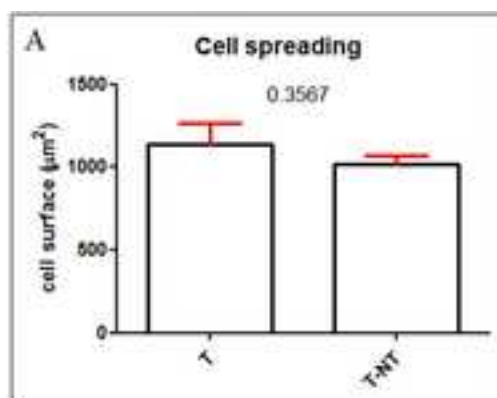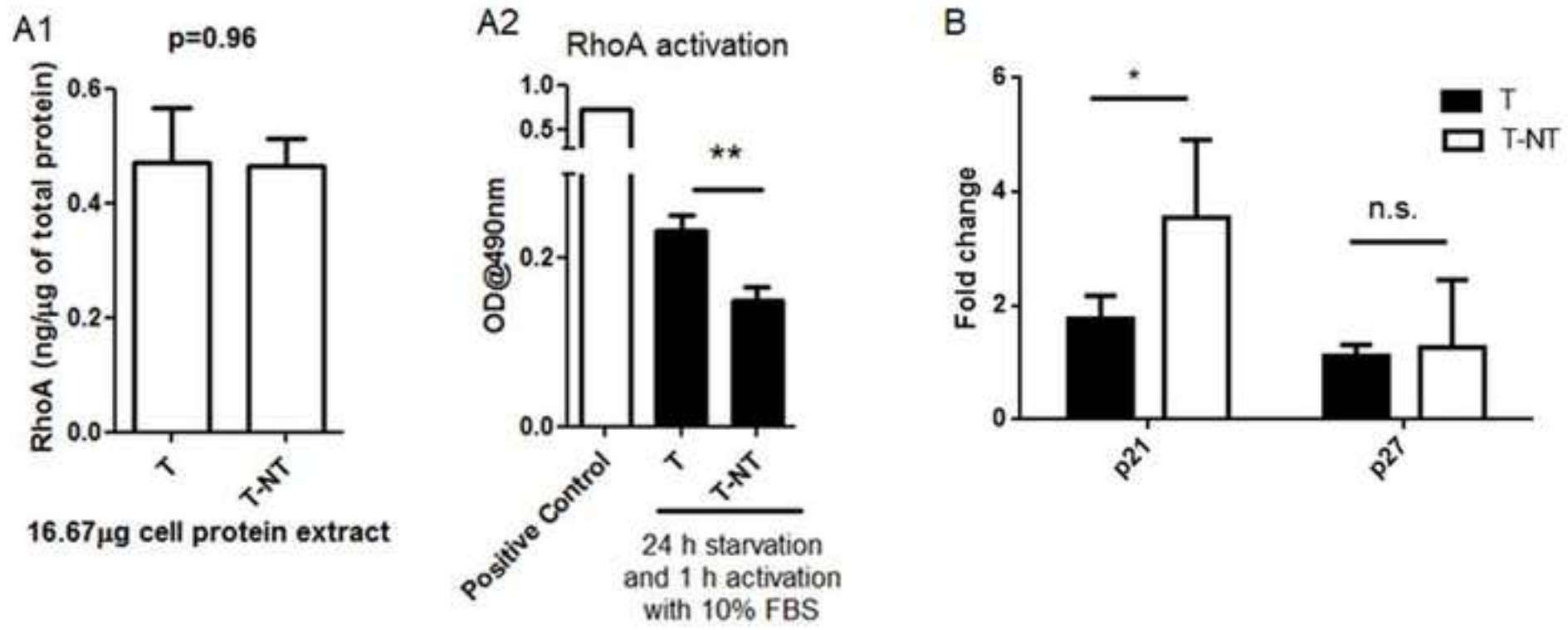**Click here to download Supplementary Material: Supplementary Materials.pdf**

NANOMEDICINE: NBM

http://www.nanomedjournal.com/
http://www.ees.elsevier.com/nano/
nanomedicine@cox.net

AUTHORSHIP AGREEMENT
Must be signed by ALL authors
Scan and upload with your submission.
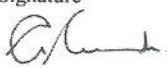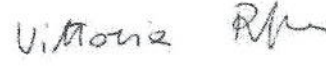
In accordance with the Authorship and Contributorship policy available at www.icmje.org, the undersigned certify that each participant: 1) made substantial contributions to conception and design, or acquisition of data, or analysis and interpretation of data; 2) drafted the article or revised it critically for important intellectual content; and 3) gives final approval of the submitted manuscript, revised versions, and version to be published. Authors should meet conditions 1, 2, and 3.

Manuscript # JN2018201
Title: Nano-topography: quicksand for cell cycle progression?

Signatures (All author names must be typed/printed next to signature. If more lines are needed, attach photocopies of this form.)

Signature	Typed name	Date
(signature)	Giovanni Signore	18/05/2018
(signature)	Alfred cuschieri	18/05/2018
(signature)	Luciana Dente	18/05/2018
(signature)	Vittoria Raffa	18/05/2018
(signature)	ELENA LANDI	18/05/2018
(signature)	MARTINA GIANNACCINI	18/05/2018
(signature)	MARIANNA SIANNINI	18/05/2018
(signature)	LIRON BERGER	18/05/2018

Note: This is not a transfer of copyright. The publisher will provide a copyright form.
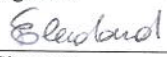
NANOMEDICINE: NBM

AUTHORSHIP AGREEMENT

Must be signed by ALL authors
Scan and upload with your submission.

In accordance with the Authorship and Contributorship policy available at www.icmje.org, the undersigned certify that each participant: 1) made substantial contributions to conception and design, or acquisition of data, or analysis and interpretation of data; 2) drafted the article or revised it critically for important intellectual content; and 3) gives final approval of the submitted manuscript, revised versions, and version to be published. Authors should meet conditions 1, 2, and 3.

Manuscript # _____

Title:

Signatures (All author names must be typed/printed next to signature. If more lines are needed, attach photocopies of this form.)

Chiara Primerano   CHIARA PRIMERANO   18/MAY/2018
Signature   Typed name   Date

_____   _____   _____
Signature   Typed name   Date

_____   _____   _____
Signature   Typed name   Date

_____   _____   _____
Signature   Typed name   Date

_____   _____   _____
Signature   Typed name   Date

_____   _____   _____
Signature   Typed name   Date

_____   _____   _____
Signature   Typed name   Date

_____   _____   _____
Signature   Typed name   Date

_____   _____   _____
Signature   Typed name   Date

_____   _____   _____
Signature   Typed name   Date

_____   _____   _____
Signature   Typed name   Date

Note: This is not a transfer of copyright. The publisher will provide a copyright form.